Mineral-specific ligand and redox dynamics of adsorbed platinum: Pathway-dependent mobility during terrestrial weathering

Emily G. Wright, Fernanda M. Loza, Elaine D. Flynn, Jeffrey G. Catalano*

Department of Earth, Environmental, and Planetary Sciences, Washington University in St. Louis, Saint Louis, MO 63130, USA

*Corresponding author: catalano@wustl.edu

Submitted to *Geochimica et Cosmochimica Acta*

September 2026

ABSTRACT

Weathering zones developed above ultramafic rocks, such as oxidized ores, soils, and laterites, concentrate the critical mineral platinum and represent a promising future resource. Prior work has documented Pt accumulation in these zones, including its common association with iron oxides. However, the fundamental mechanisms that control Pt retention versus mobilization during weathering are not well understood, inhibiting resource prediction and our knowledge of Pt environmental behavior. Dissolved platinum is predominantly complexed by chloride and ammonia in surficial waters, but the influence of these environmental ligands on Pt mobilization versus retention by mineral surfaces is currently unclear. We studied how Pt(II) aqueous speciation controls adsorption to hematite and goethite, which typically dominate the reactive mineralogy of laterites, from pH 4 to 8 and for reaction times up to 113 days. Initial speciation is the primary control on the fate of Pt, with slow ligand exchange kinetics inhibiting chemical transformations in solution even when far from equilibrium. Platinum(II)-ammine species are kinetically inert and do not appreciably adsorb to either mineral, even after several months. In contrast, Pt(II)-chloro species readily interact with both mineral surfaces. These dissolved species likely slowly convert to Pt(II)-hydroxo species in solution, further enhancing adsorption. Thus, while chloride ligands mobilize a portion of the adsorbed platinum pool, Pt(II)-ammine complexes are highly mobile and fully unreactive with iron oxide surfaces. Weathering systems hosting active biogeochemical nitrogen cycling or organic matter mineralization may thus strongly mobilize Pt. X-ray absorption spectroscopy indicates that ternary Pt(II)-chloro surface complexes form on both hematite and goethite. Over time, these adsorbed species oxidize and undergo hydrolysis on the hematite surface, but resist redox transformations on goethite. These variations indicate that Pt surface speciation will differ substantially among

weathering zones under different climate regimes, which dictate iron oxide mineralogy. Surface-mediated oxidation to Pt(IV), which occurs only in hematite-rich weathering zones, will further inhibit mineral-fluid reactions of platinum due to slower ligand exchange rates for Pt(IV) versus Pt(II) species. Such kinetic inhibition of platinum geochemical reactions will create persistent disequilibrium and result in spatially heterogeneous retention of this critical mineral at the pore scale that varies with fluid residence time.

Keywords: adsorption, platinum, iron oxides, oxidation, kinetics

1. INTRODUCTION

The projected increasing demand for platinum (e.g., Zhang et al., 2025), due to its importance as a catalyst and in medicine (Zientek et al., 2017), has resulted in its designation as a critical mineral in many countries (Deberdt et al., 2025). As one of the platinum group elements (PGEs), Pt is rare in the Earth's crust (Chen et al., 2016), with the majority of Pt currently mined from a few ultramafic layered intrusions and conduit-type deposits containing magmatic sulfides (Zientek et al., 2017)**.** However, Pt is also naturally concentrated in weathering zones formed from these primary deposits and laterites formed from ultramafic rock more broadly (Gray et al., 1996; e.g., Aiglsperger et al., 2015; Zientek et al., 2017; Oberthür, 2018). Such regolith has been proposed as a future Pt resource (e.g, Evans, 2002; Oberthür et al., 2013; Becker et al., 2014; Dzingai et al., 2021). While not currently in production, these deposits are known to host Pt concentrations as high as several mg/kg (e.g., Gray et al., 1996; Oberthür, 2018), orders of magnitude greater than the average upper continental crustal concentration of 0.8 μg/kg (Chen et al., 2016). However, the fundamental processes and mechanisms that control the enrichment or mobilization of Pt in the environment during weathering and the formation of these secondary

deposits remain poorly understood, hindering our ability to identify new resource occurrences, improve recovery methods, and predict the environmental form and fate of Pt.

Prior characterization studies provide some insight into the mineral hosts and chemical mobility of Pt during weathering. In oxidized zones derived from the weathering of ultramafic and mafic rock, Pt is distributed amongst several different mineral phases (Oberthür, 2018). While some Pt from PGE ore deposits remains bound in primary minerals during weathering (e.g., Oberthür et al., 2013), some fraction of Pt is released during weathering and becomes either associated with secondary mineral phases or leached into the broader environment (Gray et al., 1996; Locmelis et al., 2010; Oberthür et al., 2013). In particular, Pt is commonly associated with secondary iron oxides, where prior work has measured Pt concentrations of up to 3,600 mg/kg (Locmelis et al., 2010). Iron oxides are also highly abundant in laterites more broadly (e.g., Marsh and Anderson, 2011; Giorgis et al., 2014; Giovannini et al., 2017; Tauler et al., 2023; Domínguez-Carretero et al., 2024), which suggests that they could be an important phase for controlling PGEs. However, while these observations broadly suggest the chemical mobilization of Pt during weathering, the specific geochemical controls on Pt behavior are not well understood.

Existing thermodynamic data indicate that chloride, hydroxide, and ammonia are the dominant inorganic ligands complexing Pt, with the relative importance of each predicted to vary as a function of pH (Colombo et al., 2008). Chloride is predicted to form complexes with Pt under acidic pH conditions, while ammonia should be more important at circumneutral pH (Colombo et al., 2008). However, existing literature substantially disagrees on the stability of many aqueous Pt(II) species (Mountain and Wood, 1988; Wood et al., 1989; Wood et al., 1992; Sassani and Shock, 1998; Azaroual et al., 2001, 2003; Byrne, 2003). While Pt(II)-OH species are

predicted to be environmentally important (Colombo et al., 2008), proposed equilibrium constants vary by up to 10 orders of magnitude (Azaroual et al., 2001) due to uncertainty in ΔG_f^0 for Pt^{2+} (Azaroual et al., 2003). This considerable literature disagreement regarding Pt(II) thermodynamics makes it challenging to predict its speciation and underscores the importance of experimental work to evaluate platinum behavior.

Adsorption to mineral surfaces is well known to be an important control on metal mobility (Brown et al., 1999); variation in ligand concentrations and pH, resulting in changing Pt speciation, will influence complex interactions with minerals in the environment. For example, chloride mobilizes both Pd(II) and Pt(II) bound to iron oxides under weakly acidic conditions, but the degree of retention and speciation of the adsorbed metals are influenced by the relative abundance of goethite versus hematite (Wright et al., 2025; Wright et al., 2026). Platinum is also documented to sorb to kaolinite (Takahashi et al., 1999), silica (Takahashi et al., 1999; Schreier and Regalbuto, 2004), quartz (Park et al., 2005), ferrihydrite (Kubrakova et al., 2011), δ-MnO_2 (Maeno et al., 2016; Koschinsky et al., 2020), and feroxyhyte (Koschinsky et al., 2020; Li et al., 2023). However, much of this prior work has not directly explored how Pt aqueous speciation impacts adsorption behavior, particularly the role of different ligands. In addition, Pt surface speciation has only been determined for conditions relevant to weathering environments in weakly-acidic, chloride-bearing systems involving goethite and hematite (Wright et al., 2026). Other prior studies that included direct measurements of Pt surface speciation primarily focused on catalyst preparation (Muñoz-Páez and Koningsberger, 1995; Spieker et al., 2003; Hao et al., 2004; Park et al., 2005) and Pt behavior in marine environments (Maeno et al., 2016; Koschinsky et al., 2020; Li et al., 2023). These contexts involve substantially distinct (geo)chemical conditions compared to the regolith-hosted deposits that are the focus of this current study.

Further, the potential role of complexation by ammonium/ammonia in mobilizing Pt in weathering environments remains unexplored despite Pt-NH_3 species being predicted as the dominant form of Pt in many surface environments (Colombo et al., 2008). The effects of circumneutral pH, which occurs deeper in weathering zones (e.g., Thompson and Rodgers, 1977; Fandeur et al., 2009; Ito et al., 2021), and other complexing ligands on Pt binding to iron oxides have yet to be characterized, limiting our understanding of Pt behavior in terrestrial weathering environments.

Most metals undergo fast ligand exchange in solution (Lincoln and Merbach, 1995; Richens, 2005), enabling accurate prediction of aqueous species based on equilibrium thermodynamics. However, equilibrium behavior may not be a valid assumption for Pt in all environments. Ligand exchange rates for Pt(II) species are known to have half-lives varying from hours to decades, four to eight orders of magnitude slower than for analogous Pd(II) species (Gröning and Elding, 1989; Brønnum et al., 1992; Lincoln and Merbach, 1995; Richens, 2005). Slow coordination kinetics may have influenced past experimental results (Takahashi et al., 1999; Turner et al., 2006; Cobelo-García et al., 2008). For example, a prior study observed faster uptake after pre-mixing Pt with river water for 60 hours compared to simultaneous introduction of water and sediment (Turner et al., 2006), implying that slow aqueous reactions may influence adsorption behavior. Prior work studying Pt environmental behavior has only measured adsorption over short timespans, at most several weeks (Takahashi et al., 1999; Turner et al., 2006; Kubrakova et al., 2011; Maeno et al., 2016; Koschinsky et al., 2020; Li et al., 2023); however, several months at minimum are required for Pt aqueous speciation to equilibrate (Elding, 1970), with some specific Pt species likely equilibrating over years to decades (Brønnum et al., 1992; Torapava et al., 2013). Thus, it is currently unclear how much these prior

studies model transient behavior or accurately model geochemical processes. Furthermore, the potential evolution of Pt in the environment over longer timespans has not been previously investigated.

In order to better understand the fundamental controls on Pt(II) behavior in the environment, adsorption to hematite and goethite across a range of experimental conditions was studied. All experiments were conducted with Pt(II) because it is predicted to be the dominant redox state in freshwater systems (Cobelo-García et al., 2013). While dissolved O_2 has been demonstrated to oxidize $Pt(OH)_4^{2-}$ (Wu et al., 1990) at high pH (1 M NaOH), prior investigations of Pt(II)-Cl species at low pH (0.5 M $HClO_4$) have not demonstrated the formation of any Pt(IV) species for solutions in contact with air (Elding and Leden, 1966; Elding, 1970). The effects of chloride and ammonia on Pt adsorption were evaluated across a pH range of 4 to 8 in order to assess the relative effect of complexing ligands, including with different initial Pt(II) speciation. Kinetic studies were also performed at pH 6 in order to track initial uptake and investigate temporal effects on Pt(II) behavior. These laboratory experiments were complemented with X-ray absorption spectroscopy (XAS) to elucidate the identity of bound Pt and assess possible ternary surface complexation in order to improve our understanding of the molecular-scale mechanisms that control the fate of Pt in the environment.

2. MATERIALS AND METHODS

2.1 Mineral Synthesis and Characterization

Hematite and goethite were synthesized using adapted versions of forced hydrolysis procedures (Schwertmann and Cornell, 2000). Both of these adapted methods were previously described by Wright et al. (2026). For hematite synthesis, 300 mL of a 1 M NaOH solution was

slowly added to a continuously stirred 500 mL solution of 0.2 M $Fe(NO_3)_3 \cdot 9H_2O$. After this first addition, 50 mL of 1 M $NaHCO_3$ was slowly added. The synthesis fluid and resulting suspension was then aged at 98°C for five days. For goethite synthesis, 50 mL of 1 M $Fe(NO_3)_3 \cdot 9H_2O$ was slowly added to a continuously stirred 90 mL solution of 5 M KOH. The solution was diluted to 1 L with ultrapure water (18.2 MΩ cm), with the pH measured to ensure it was above 13. The resulting fluid and solids were aged at 70°C for 60 hours.

After aging, the resulting solids from both synthesis methods were rinsed with at least 450 mL ultrapure water via vacuum filtration (0.45 μm MCE filter for hematite, 0.22 μm MCE filter for goethite) in order to remove excess dissolved ions. The resulting wet pastes were resuspended with additional ultrapure water and stored in aluminum foil-wrapped polypropylene bottles and thoroughly mixed prior to any subsampling. Suspension concentrations were determined gravimetrically. Multiple batches of hematite and goethite were used for experiments (**Table S1**).

For mineral characterization purposes, a subsample of each mineral suspension was dried overnight in a convection oven (70°C for hematite, 55°C for goethite). X-ray diffraction (XRD) patterns of each batch were collected with a Bruker d8 Advance Diffractometer using Cu Kα radiation to ensure the purity of the synthesis (**Fig. S1**). Additional details regarding the data collection parameters for the XRD patterns are provided in the **Supplementary Material**. The Brunauer-Emmett-Teller (BET) specific surface area of each mineral batch (**Table S1**) was determined by collecting N_2 gas adsorption isotherms using a Quantachrome Nova 2000e after degassing under vacuum for at least 18 hours at room temperature (goethite) or 100°C (hematite).

2.2 pH Adsorption Edge Experiments

The effects of pH and complexing ligands on Pt(II) adsorption to hematite and goethite were investigated by constructing pH adsorption edges between pH 4 and 8 in the presence of variable amounts of chloride and ammonia. This pH range was chosen to reflect the relevant range of pH conditions in weathering zones and environmental systems more broadly (Baas Becking et al., 1960; Thompson and Rodgers, 1977; Fandeur et al., 2009; Ito et al., 2021). Note that below pH ~9.2, ammonium (NH_4^+) is the actual chemical form of ammonia (NH_3) in solution; the term "ammonia" is used through this study to refer to both species. Experiments were conducted for both goethite (1 g/L) and hematite (2 g/L) in fluids containing 50 μM Pt (~9.8 mg/L). Prior work has shown that dissolved Pt concentrations in the environment may be in the low ng/L (Mashio et al., 2016) and as high as 2.8 μg/L in waters near a PGE ore deposit (Coker et al., 1991); substantially elevated concentrations of Pt were used in experiments to ensure dissolved Pt remained quantifiable after adsorption with available instrumentation. Adsorption was measured in solely 2 or 10 mM total chloride or 10 mM total chloride with either 0.25 mM ammonia (hematite only) or 10 mM ammonia (both minerals). These chloride concentrations were chosen to align with previous work to enable more direct comparison (Wright et al., 2025; Wright et al., 2026) and be consistent with a range of chloride concentrations measured in relevant natural systems (McGregor et al., 1998; Alexander et al., 2017; Ahokpossi et al., 2018; Molekoa et al., 2019). There is less data on relevant ammonia concentrations, but Colombo et al. (2008) used a value of 0.5 mM for calculation of Pt speciation based on prior literature (Roney et al., 2004). Based on preliminary experiments, 10 mM was chosen to represent a maximum endmember condition to assess the specific impact of ammonia and because modeling this condition using thermodynamic data suggest that Pt-NH_3 species should dominate at pH 5 and above (**Fig. 1**) (Mountain and Wood, 1988; Wood et al., 1989).

Initial experiments were performed with a 2.5 mM Pt stock solution that was prepared by dissolving sodium tetrachloroplatinate(II) hydrate in ultrapure water. This resulted in a solution that contained Pt(II)-chloro species. Based on preliminary experiments and literature data suggesting the importance of kinetics, the effect of initial Pt(II) coordination on Pt adsorption behavior was assessed by repeating the 10 mM chloride and 10 mM ammonia pH edge for both minerals with a 3 mM Pt stock solution prepared by dissolving tetraammine platinum(II) nitrate in ultrapure water, resulting in a solution of Pt(II)-ammine species. Other than the initial Pt coordination, these experiments were identical. All stocks were prepared with reagent-grade chemicals. Chloride and ammonia were added through the addition of dissolved NaCl and NH_4NO_3, respectively, accounting for the chloride or ammonia contribution from the Pt stock solution.

The pH of each sample was measured and adjusted by addition of small aliquots of HNO_3 and NaOH solutions prior to and after adding the Pt stock solution, as well as at 3-5 and 21 hours into the experiments, to ensure it was within 0.05 units of the target pH. A double-junction pH electrode setup containing 3 M KNO_3 as the outer chamber electrolyte, initially described by Wright et al. (2025), was used to prevent excess chloride addition to the samples. In order to better control the pH of samples, 1 mM MES buffer was used for pH 5 and 6 samples and 1 mM MOPS buffer was used for pH 7 and 8 samples. No buffer was added to the pH 4 samples because there are no known Good's buffers that are effective at that low pH (Ferreira et al., 2015). Triplicate samples were prepared at pH 6. Corresponding mineral-free controls for all pH values investigated were used to monitor for pH-dependent solubility. After 24 hours of reaction time, the final pH was recorded and the samples were centrifuged (3398 g for 20 minutes) and filtered (0.22 μm MCE syringe filter). A portion of each sample was acidified to 2% HNO_3 (trace

metal grade) for analysis of Pt by inductively-coupled plasma optical emission spectroscopy (ICP-OES) using a Thermo iCAP 7400 DUO ICP-OES (1 ppm Sc internal standard) in axial mode. Adsorbed Pt was calculated by difference, using the pH-specific mineral-free controls as the starting Pt concentration, and normalized to the available surface area. Error was determined by adding in quadrature the average error from the weighted calibration curve, the relative standard deviation from physical triplicate (pH 6) samples, and the relative standard deviation from triplicate instrumental measurements. In a few experiments prepared with the Pt-NH_3 species, the measured final dissolved Pt concentration was slightly greater than the calculated initial concentration, resulting in negative apparent adsorption with values of -0.004 to -0.16 $\mu mol/m^2$. These slightly negative adsorption values are likely the result of systematic error resulting from the actual initial Pt concentration being greater than the calculated value. For visualization purposes, these values were set to 0.

2.3 Kinetic Experiments

Initial pH-edge experiments and previous literature (e.g., Turner et al., 2006; Cobelo-García et al., 2007) suggested that slow Pt kinetics may result in non-equilibrium behavior within 24 hours. In order to assess this possibility, a set of large volume samples were prepared for short-term (120 mL in 125 mL Nalgene bottles) and longer-term (140 mL in 250 mL Nalgene bottles) kinetic experiments at pH 6, the midpoint of the pH range previously assessed. For both goethite (1 g/L) and hematite (2 g/L), four experimental conditions were evaluated: 10 mM chloride with Pt-Cl stock; 10 mM ammonia with Pt-NH_3 stock; 10 mM chloride and 10 mM ammonia with Pt-Cl stock; and 10 mM chloride and 10 mM ammonia with Pt-NH_3 stock. The short-term kinetic reactors only used the Pt-Cl stock conditions, based on results from the pH edge experiments. Mineral batches differed between some experiments (**Table S1**).

The general experimental procedure initially followed that previously described (**Section 2.2**); at dedicated timepoints, a 10 mL subsample was extracted and filtered (0.22 μm MCE syringe filter). Subsamples from the longer-term kinetic reactors were centrifuged (3398 g for 8 minutes) prior to filtration, while the short-term samples were directly filtered. In the short-term reactors, subsamples were periodically collected from 0.25 to 72 hours. The longer-term reactors were subsampled from 1 to 113 days. All experimental reactors were stored on a shaker table at 180 rpm; prior to subsampling, reactors were thoroughly mixed on a stir plate for several minutes. The pH of each reactor at each timepoint was recorded; after removing a subsample, the pH was adjusted to back within the desired range if it had drifted beyond pH 6±0.05. Over the course of all experiments, none of the reactors drifted beyond pH 6±0.20. A set of mineral-free controls using the same experimental conditions were also prepared to track the possibility of slow precipitation. After filtering, the subsamples were acidified for Pt measurement by ICP-OES as described previously. Not all subsamples containing the Pt-NH_3 stock were measured. Adsorption was determined by difference, using the Pt concentration measured in the associated mineral-free reactor at the first time point as the starting concentration. Error was calculated in the same manner as the pH-edge experiments, but there were no physical triplicates. Reaction time was defined as the timespan between when Pt was initially added to the reactors and when the subsamples were filtered.

2.4 X-ray Absorption Spectroscopy

XAS was used to better understand Pt oxidation state and binding configurations on the hematite and goethite surfaces. Samples of Pt adsorbed to hematite and goethite with 10 mM chloride and the Pt-Cl stock at pH 6 and 8 were prepared following the same general procedure as the pH edge experiments (**Section 2.2**). Analogous samples at pH 4 were previously published

(Wright et al., 2026). The potential role of kinetics and ammonia in Pt surface speciation was assessed by preparing multiple samples under identical chemical conditions (10 mM chloride, 0 or 10 mM ammonia, pH 6, Pt-Cl stock) at different experimental timepoints. These samples were prepared similarly to the macroscopic kinetic experimental samples described in **Section 2.3**. For all XAS samples, sample sizes and mineral loadings were scaled (50 mL total volume, up to 8 g/L) in order to produce enough solids for analysis. Total Pt concentrations were chosen to attempt to replicate the adsorbed Pt concentrations previously measured in macroscopic experimental samples. Detailed sample information is provided in **Table S2**. After reaction for the specified time, the samples were centrifuged (3398 g for at least 10 minutes) and the solids were collected as a wet paste for analysis and sealed in aluminum sample holders using Kapton tape. In order to prevent possible reduction of Pt, only plastic tools were used. For hematite samples, all of the supernatant was decanted after centrifugation and the wet mineral paste was scraped out of the 50 mL conical tubes using plastic disposable spatulas and then packed in the sample holder. For goethite samples, the majority of the supernatant was decanted, leaving no more than 15 mL behind. The goethite was then resuspended to create a more concentrated suspension, which was then filtered onto a 0.22 μm MCE filter membrane. The wet mineral paste was scraped off the filter membrane and packed in the sample holder. All prepared samples were immediately stored at -80°C and transported to the beamline in a liquid N_2 dry shipper to prevent desiccation or further reaction. The supernatant was filtered with 0.22 μm MCE syringe filters and analyzed for total dissolved Pt after acidifying using the method described previously.

Several Pt solids ($PtCl_2$, PtO_2, $PtCl_4(NH_4)_2$, and $PtCl_6(NH_4)_2$) were prepared as reference standards. A mortar and pestle was used to grind and mix the solids with cellulose to an appropriate dilution. The resulting powders were packed in aluminum sample holders with

Kapton tape before shipping to the beamline at room temperature. An additional Pt reference ($Pt(O_2C_5H_7)_2$) was prepared by grinding the solid with a mortar and pestle and spreading the resulting fine powder on Scotch tape.

XAS spectra of Pt adsorbed to goethite and hematite were collected at beamline 6-BM at the National Synchrotron Light Source II (NSLS-II), Brookhaven National Laboratory. The incident beam energy was controlled with a cryogenically-cooled Si (111) double-crystal monochromator with a harmonic rejection mirror. Platinum L_3-edge fluorescence-yield data of experimental samples were collected at 78 K (Linkham cold stage). Data on initial samples (HCl-pH4, HCl-pH8, HCl-d1, GCl-pH4, GCl-pH8, GCl-d1) were collected with a 7-element Si drift detector; all remaining data were collected with a 4-element Si drift detector. Spectra from the Pt standards were collected in transmission mode at room temperature. Multiple scans were averaged with Athena (Ravel and Newville, 2005). Due to shifts between individual scans, all scans from an individual sample were aligned prior to averaging. Spectra were energy calibrated to 11564 eV using scans of a Pt metal reference foil.

Linear combination fitting (LCF) of the normalized Pt L_3-edge X-ray absorption near edge structure (XANES) spectra was conducted in Athena (Ravel and Newville, 2005) to assess possible changes in oxidation state. The Pt L_3-edge position does not shift in energy substantially with a transition from Pt(II) to Pt(IV), but this oxidation state change does induce an increase in the white line height (**Fig. S2**). Additionally, the white line and edge position are sensitive to coordinating ligand, with O neighbors resulting in a taller white line compared to Cl neighbors (**Fig. S2**). All XANES spectra were fit as a linear combination of four possible components: $Pt(O_2C_5H_7)_2$ for Pt(II) bound to O; $PtCl_4(NH_4)_2$ for Pt(II) bound to Cl; PtO_2 for Pt(IV) bound to O; and $PtCl_6(NH_4)_2$ for Pt(IV) bound to Cl. Individual components were allowed to vary freely

and the sum of components was not constrained to equal one. Components that were negative or within error of 0 were discarded from the fit; the Pt(IV)-Cl component was not present in any sample. The fractions of Pt(II) and Pt(IV) were determined by summing each Pt(II) and Pt(IV) component and dividing the total sum of the LCF.

For analysis of the EXAFS spectra, local structural models were refined in SixPACK. The backscattering phase and amplitude functions used for fitting were generated with FEFF8L (Ankudinov et al., 1998) in Larch (Newville, 2013) using the modified version of the crystal structure of *trans*-$[PtCl(OH)(NH_3)_2]\cdot H_2O$ (Arpalahti et al., 1994) that was previously described (Wright et al., 2026). Briefly, a Pt neighbor at 3.328 Å was replaced with a Fe neighbor in order to calculate theoretical Pt-Fe scattering paths. Based on fitting of a spectrum of Pt foil, an amplitude reduction factor (S_0^2) of 0.94 was used. Given the possibility of oxidation, which would result in a transition from square-planar to octahedral geometry, our prior assumption of constraining the first shell paths to sum to a coordination number (CN) of 4 (Wright et al., 2026) was no longer a valid approach. Instead, the CN of the first shell paths, Pt-Cl and Pt-O, were allowed to vary freely and the mean-square displacement (σ^2) was instead constrained. Based on fitting of known standards (**Fig. S3**; **Table S3**), σ^2 for both paths was set to 0.0026 $Å^2$. Additionally, to fit additional features beyond the first shell, multiple Pt-Fe paths were included, with a single σ^2 (0.005) used for all paths. Given the potential change in coordination geometry, no multiple scattering paths were included. A single ΔE_0 was fit for all paths. Spectra were fit in R-space from 1.1 to 4.5 Å using the Fourier transform *k*-range from 3.0 to 12.3 $Å^{-1}$. Since this structural model differed from our previous work, select previously published spectra (Wright et al., 2026) were refit in order to enable more direct comparison of fitting results.

3. RESULTS

3.1 Fluid Composition Effects on Macroscopic Pt Binding

For both hematite and goethite, substantial adsorption occurs within 24 hours across the entire pH range studied (4 to 8; **Fig. 2**) when the initial speciation consists of Pt-Cl complexes. However, the pH dependence of Pt adsorption differs between the minerals. For hematite, Pt adsorption clearly increases with increasing pH, with the largest amount of adsorption observed at the upper pH range tested (7-8; **Fig. 2a**). In contrast, Pt adsorption on goethite is largely pH invariant (**Fig. 2c**). Additionally, consistently greater Pt adsorption is observed on goethite (up to ~1.8 μmol/m^2) compared to hematite (up to ~1.1 μmol/m^2) (**Fig. 2**). Decreasing the chloride concentration from 10 to 2 mM results in a slight increase in adsorption at pH ~5 and below, although this effect is clearer for hematite (**Fig. 2**). The addition of ammonia results in no measurable difference in the amount of adsorption observed when reactors were prepared with Pt-Cl complexes (**Fig. 2**).

However, negligible adsorption occurs within 24 hours when starting with Pt-NH_3 species (**Fig. 2**). The strong divergence in adsorption behavior across reactors prepared with the same bulk composition (10 mM chloride and 10 mM ammonia) but different initial Pt speciation (Pt-Cl species versus Pt-NH_3 species; **Fig. 2**) is a clear sign of non-equilibrium behavior. A prior preliminary experiment with Pt-NH_3 complexes that was chloride free also consistently resulted in negligible adsorption at pH 7±0.05 (**Fig. S4**), regardless of the amount of ammonia present.

3.2 Effects of Kinetics of Macroscopic Pt binding

The pH adsorption edge experiments display non-equilibrium behavior for a 24-hour reaction time because distinct outcomes occur under identical system compositions. This pathway-dependence indicates that kinetics affected by initial Pt(II) coordination may play an

373 important role in controlling Pt behavior. Two separate kinetic experiments were conducted to
374 assess variability in Pt uptake over time: a shorter-term kinetic experiment was used to assess
375 initial Pt uptake rates and a separate longer-term kinetic experiment was conducted to evaluate
376 the possible temporal evolution of Pt uptake. Based on the results of the 24-hour experiments
377 (**Fig. 2**), Pt-NH_3 species were only used for longer-term kinetic experiments to assess to
378 possibility of slow adsorption.
379 Uptake for systems initially containing Pt-Cl species is rapid to both minerals, with the
380 majority occurring within the first 15 minutes (**Fig. S5**). In both shorter- and longer-term kinetic
381 experiments, the amount of adsorption continues to evolve after 24 hours (**Fig. 3,S5**).
382 Quantitative differences in uptake rate between the shorter- and longer-term kinetic reactors are
383 likely attributable to differences in experimental design (**Supplementary Material**).
384 Adsorption in reactors with initially Pt-Cl species continues to evolve over several
385 months (**Fig. 3**), with the eventual trend in uptake controlled by the presence of ammonia. When
386 no ammonia is present, adsorption continues to increase over time (**Fig. 3**). However, while
387 ammonia has no apparent effect in the shorter-term kinetic reactors that were subsampled for up
388 to 3 days, Pt adsorption in the mixed Cl-NH_3 longer-term reactors starts to plateau after about a
389 week (**Fig. 3,S5**). In sharp contrast, negligible adsorption occurs over all time periods when Pt
390 initially occurs as Pt-NH_3 species, regardless of the presence of chloride (**Fig. 3**).
391 In the mineral-free control reactors prepared with Pt-Cl complexes, there is a small drop
392 in Pt concentrations over long time periods, possibly due to adsorption to reactor walls (**Fig. S6**).
393 In the mixed Cl-NH_3 reactor, a small amount of precipitation occurred sometime between day 17
394 and 22 of the experiment (**Fig. S6**). The resulting precipitate was not visible in the original
395 reactor bottle, but could be seen as a fine dark powder after centrifugation. This may be the

formation of one of the Magnus salts, which are known to form from the mixing of ammonia with $PtCl_4^{2-}$ (Atoji et al., 1957). The Pt concentration remaining in solution after this precipitation event (~40 μM; **Fig. S6**) is still substantially in excess of Pt concentrations in the corresponding mineral-containing reactors (<10 μM; **Fig. 3**). Thus, while at least some of the reactors may have been initially supersaturated with respect to Pt, rapid adsorption quickly decreased dissolved Pt concentrations. No substantial change in Pt concentrations were detected in the mineral-free reactors prepared with Pt-NH_3 species, regardless of the presence of chloride (**Fig. S6**).

3.3 Surface Coordination State

The macroscopic results from benchtop experiments indicate that the amount of adsorbed Pt is strongly influenced by initial Pt(II) speciation, pH, iron oxide mineralogy, ligands present, and reaction time (**Fig. 2,3**). However, these data alone do not provide adequate constraints on the underlying mechanisms. Further, modeling to assess the impact of aqueous speciation is not feasible given substantial disagreements in Pt thermodynamic data (e.g., Azaroual et al., 2001). Thus, direct measurement of Pt surface speciation using XAS is necessary to identify the mechanisms controlling Pt retention by iron oxide surfaces. The effect of pH after 24 hours of aging and the effect of aging time, as well as the presence of ammonia, at pH 6 were evaluated. All XAS samples were prepared with Pt-Cl complexes, due to the lack of uptake with Pt-NH_3 complexes (**Fig. 2,3**).

For all samples, the Fourier transform magnitudes of the EXAFS spectra have one large, sometimes asymmetric feature from approximately 1.3 to 2.3 Å (R+ΔR) (**Fig. 4b**), consistent with a mixture of O and Cl neighbors at ~2.0 and ~2.3 Å, respectively (Maeno et al., 2016; Koschinsky et al., 2020; Wright et al., 2026). Variations in the spectra are primarily due to shifting of this feature (**Fig. 4**), indicating differences in the O and Cl CN. Smaller variations in

the Fourier transform occur between R = 2.5 to 4 Å (R+ΔR) (**Fig. 4**) and likely reflect a mixture of multiple-scattering contributions and signal from second shell Fe neighbors.

A FEFF-based structural model was developed to evaluate Pt binding variations on hematite and goethite surfaces. The first coordination shell was modeled as a mixture of O and Cl neighbors at ~2.0 and ~2.3 Å, which were allowed to vary freely. The σ^2 value for both first shell paths was fixed to 0.0026 $Å^2$, based on fitting of known standards (**Supplementary Material**). In order to fit features at intermediate distances, three separate Pt-Fe paths were included with inter-atomic distances of ~3.08, ~3.68, and ~3.87 Å, similar to our prior study (Wright et al., 2026). The first distance corresponds to an edge-sharing coordination, while the two longer distances are consistent with either a monodentate or corner-sharing bidentate configuration. To decrease parameter correlations, a single σ^2 value (0.005 $Å^2$) was fixed for all Pt-Fe paths.

For hematite samples, increasing pH results in weakening of oscillations in the EXAFS spectra between k = 8.5 to 12 $Å^{-1}$ (**Fig. 4**). Oscillations in this region, as well as below k = 5 $Å^{-1}$, increase in magnitude with longer reaction time at pH 6 (**Fig. 4**). Spectra of Pt adsorbed to hematite in the presence of ammonia are similar to ammonia-free samples reacted for the same amount of time (**Fig. 4**). Principal component analysis (PCA) of all hematite spectra indicates that ~97% of the total variance is explained by three components, with the indicator (IND) value also minimizing on this component (**Table S4**). Reconstructions with three components broadly reproduce the hematite EXAFS spectra, although there may be some additional variability not captured (**Fig. S7**). This spectral variability observed indicates that Pt surface speciation is sensitive to pH and evolves over time.

441 The structural model developed reproduces the hematite spectra well (**Fig. 4**). The fits
442 yield between 1.7 and 5.2 O neighbors; Cl neighbors vary between 0.3 and 2.7 (**Table 1**).
443 Increasing pH and reaction time both result in adsorbed Pt becoming coordinated to an
444 increasing number of O neighbors and fewer Cl neighbors (**Table 1; Fig. 5**). The presence of
445 ammonia does not measurably change the fitting results (**Table 1**). A shift from aquo or hydroxo
446 ligands to ammine ligands would produce subtle shifts in the EXAFS spectra from slight
447 differences in Pt-O versus Pt-N interatomic distances, slight changes in backscattering phase, and
448 weakening of backscattering amplitude. However, the series of spectra and associated structural
449 model fits are identical with and without ammonia (**Table 1; Fig. 4,5**), suggesting that NH_3 does
450 not influence Pt surface speciation on hematite.
451 For all hematite samples, the number of Fe neighbors at corner-sharing distances (~3.68
452 and ~3.87 Å) are substantially greater than at an edge-sharing distance (~3.08 Å). However,
453 changes in the first shell coordination could also result in changes in the number of second shell
454 Fe neighbors due to a possible shift in binding geometry. For example, the O CN is well
455 correlated with the number of Fe neighbors at ~3.08 Å (R^2 = 0.6046 for hematite; **Fig. S8**). This
456 could reflect a greater preference for edge-sharing geometries for Pt-O surface species or it may
457 be a fitting artifact due to interference from the decreasing intensity of the Pt-Cl path. The
458 second interpretation is more likely because such a change in the O CN does not correspond to a
459 decrease in Fe neighbors at longer, corner-sharing distances; there is no correlation (**Fig. S8**).
460 The total number of Fe neighbors is largely insensitive to O CN (**Fig. S8**), indicating that Pt-O
461 surface species are not more coordinated to the surface. These observations suggest that the Pt
462 binding geometry does not dramatically shift with different coordinating ligands. However, the
463 number of Fe neighbors (**Tables 1,2; Fig. S8**), particularly at longer Pt-Fe distances are

unrealistically large. This is possibly an artifact of the large σ^2 (0.005 $Å^2$) used to constrain these Fe neighbors; it was not possible to independently constrain this value. Additionally, unlike our previous model (Wright et al., 2026), no multiple-scattering paths were included because changes in the XANES spectra suggest that square-planar Pt(II) has oxidized to octahedral Pt(IV) (**Fig. 6; Section 3.4**) and accurately constraining multiple-scattering path geometries for co-occurring octahedral and square-planar coordination states was not feasible. However, this assumption, as well as the choice for second shell σ^2, likely results in overestimation of the Fe CNs, particularly when a greater fraction of Pt occurs as square-planar Pt(II). To assess this possibility, samples HCl-pH4 and GCl-pH4 were refit using our previous model approach including multiple-scattering (Wright et al., 2026), but with an updated S_0^2 to 0.94 and the second shell σ^2 set to 0.005 $Å^2$ (rather than 0.002 $Å^2$). Compared to the main fit approach presented in this study (**Tables 1,2**), these alternative fits yield parameters for the Fe neighbor at ~3.08 Å within error of values in our primary model but results in smaller coordination numbers for the Fe neighbors at ~3.68 and ~3.87 Å (**Table S5**). This assessment supports the assertion that the number of Fe neighbors is likely overestimated by the primary fitting approach because multiple-scattering was not accounted for in that model. Still, the observations of a preference for edge-sharing binding geometries and the overall insensitivity of binding geometry to the first shell coordination remain robust.

In contrast, the set of all EXAFS spectra for Pt adsorbed to goethite with 24-hour reaction times are essentially indistinguishable, regardless of the pH or presence of ammonia (**Fig. 4**). There is also little change in the goethite spectra for longer aging times, other than a possible subtle increase in oscillations above 11 $Å^{-1}$ (**Fig. 4**). A PCA of all goethite spectra indicates that ~97% of the total variance is explained by two components, with the IND value also minimizing

on the second component (**Table S6**). The minimal variability in the goethite EXAFS spectra suggests that Pt surface speciation is largely the same across all goethite samples, in contrast with Pt adsorbed to hematite.

The structural model developed for the goethite samples well reproduces the spectra (**Fig. 4**). This fitting model identifies between 2.3 and 3.0 O neighbors and 1.7 and 2.3 Cl neighbors for the series of goethite spectra (**Table 2**). Increasing pH does not change the first coordination shell fits within error (**Fig. 5; Table 2**). Longer reaction times result in a slightly greater O CN and lower Cl CN, but these values are within error for the chloride-only samples (**Fig. 5; Table 2**). For samples of Pt adsorbed to goethite with both chloride and ammonia, the general trend is the same, although the resulting CNs are not quite within error between 1 and 57 days (**Table 2**), suggesting that NH_3 does not substantially influence Pt surface speciation on goethite. These fitting results indicate that Pt surface speciation on goethite is largely invariant, regardless of pH or aging time. Similar to hematite, Pt adsorbed to goethite displays a preference for corner-sharing geometries (**Table 2**). The number of Fe neighbors for Pt adsorbed to goethite is within error of the number fit to Pt adsorbed to hematite (**Tables 1,2; Fig. S8**), indicating that Pt surface binding geometries are similar on both minerals.

For all samples, LCFs of the XANES region allow for an alternative estimation of the O CN and Cl CN. The resulting XANES-derived O CN well correlates with the EXAFS-based O CN fit ($R^2 = 0.9401$) but more poorly correlates with quantification of Cl CN ($R^2 = 0.7467$; **Fig. S9**). While the XANES-derived CNs are not consistently within error of the EXAFS-derived CNs, the general trends identified with EXAFS fitting (little change in goethite coordination and progressive loss of Cl ligands and increasing O CNs on hematite) remain robust with XANES LCFs.

3.4 Oxidation State of Adsorbed Pt

As noted above, fitting of the hematite EXAFS spectra indicates an average first-shell coordination number greater than 4 for multiple samples (**Table 1; Fig. 5**), suggesting a shift from square-planar to octahedral geometry that accompanies oxidation of Pt(II) to Pt(IV). Similarly, variability in the height of the white line in the XANES region (**Fig. 6**) also indicates that oxidation occurred in at least some samples. To quantitatively assess oxidation, two complementary fitting approaches were taken using the EXAFS and XANES spectra.

Analysis of the EXAFS spectra show that aging results in an increasing number of first shell neighbors on hematite, but no such change on goethite (**Fig. 5e**). Changing pH has no effect on the number of first shell neighbors. These changes in the number of first shell neighbors provide a constraint on the average coordination state and thus oxidation state: square planar Pt(II) has 4 neighbors while octahedral Pt(IV) has 6. Although this EXAFS-based approach has large errors due to fitting uncertainties, it indicates that Pt gradually oxidized over time on hematite but displays a stable oxidation state on goethite (**Fig. 7a**). For both minerals, changing pH does not result in statistically different degrees of Pt oxidation (**Fig. 7b**). However, this approach does identify the presence of at least a small amount (20-30%) of an octahedral component occurring in every sample (**Fig. 7a,b**). This could indicate that some Pt(II) has oxidized in all reactors, even after only 24 hours. Alternatively, this result could be an artifact of the fitting approach. For example, a decrease in the first shell σ^2 value would result in a decrease in the fitted CN values and thus the calculated oxidation state. The EXAFS fitting approach applied σ^2 value derived from fits to Pt standards with known structures (**Supplementary Material**). However, smaller σ^2 values were obtained for PdO and $PdCl_2$ (Wright et al., 2025), analogous square-planar compounds. This suggest that square-planar Pt(II) compounds may have

a very rigid first shell and that our obtained σ^2 values from the Pt standards may be overestimated because of systematic errors in the measurements or FEFF calculations. A smaller σ^2 value would result in smaller CNs and thus a lower calculated oxidation state. Such systematic biases from the choice of σ^2 are not captured in the fitting uncertainties because they are not statistical in nature. Thus, while the trends in oxidation state observed with this fitting approach are informative, the quantitative values produced are highly sensitive to model choices during fitting.

An alternative fitting approach to assess oxidation state uses the XANES region. As previously discussed (**Section 2.4**), the height of the white line for a Pt L_3-edge spectrum is sensitive to both oxidation state and coordinating ligand (**Fig. S2**). For goethite spectra, the white line subtly increases with increasing reaction time, but is insensitive to changing pH (**Fig. 6**). In contrast, increasing pH and reaction time both result in a taller white line for hematite spectra, a much larger change than observed for goethite (**Fig. 6**). The white line intensity is affected by both changes in the number of O versus Cl neighbors and a change in the average oxidation state (**Fig. S2**). A LCF was conducted using standards of Pt(II) and Pt(IV) coordinated to O and Cl. The resulting components were then used to determine the amount of Pt(IV). For all samples, no Pt(IV)-Cl component was obtained during fitting. The resulting LCFs reproduce changes in the white line for all spectra (**Fig. S10**).

For all but one sample (HCl-d13), the amount of Pt(IV) determined by XANES LCF (**Table 3**) is within error of the value obtained with the EXAFS-based coordination geometry approach (**Fig. 7**). On hematite, increasing reaction time results in greater Pt oxidation, but no such change is observed on goethite (**Fig. 7**). Similarly, increasing pH results in a slightly larger oxidized component on hematite but not on goethite (**Fig. 7d; Table 3**), a trend that is

qualitatively captured with the EXAFS-based approach but obscured by large error values (**Fig. 7b**). The presence of ammonia results in a greater Pt(IV) component at 1 day of aging compared to chloride-only samples, but at longer aging times the Pt(IV) component is within error or smaller than the chloride-only sample (**Fig. 7c; Table 3**). Similar to the EXAFS-based approach, the XANES LCFs result in a small Pt(IV) component in all samples (~20%), suggesting that some oxidation may have occurred in all reactors.

4. DISCUSSION

4.1 Persistent Disequilibrium of Adsorbed Platinum

Our experimental results demonstrate that adsorbed and dissolved Pt do not equilibrate over a several month period. The addition of dissolved ammonia produces negligible effects on Pt adsorption over the first several days of reaction for solutions initially containing Pt-Cl complexes (**Fig. 2,3**), despite existing thermodynamic data predicting that $Pt(NH_3)_4^{2+}$ should be the dominant form of Pt at circumneutral pH (**Fig. 1**). Over longer timescales (months), adsorption continues to evolve for systems with Pt introduced as chloride complexes (**Fig. 3**), both in the absence and presence of ammonia. Experiments with the same bulk fluid composition but instead prepared with $Pt\text{-}NH_3$ initial species display unmeasurable adsorption for all timescales studied (**Fig. 2,3**). This divergent behavior in systems with identical fluid compositions demonstrates a clear pathway-dependence controlled by initial Pt speciation. If the aqueous species had reached equilibrium, then Pt adsorption should be consistent (within error) irrespective of its starting chemical form. These observations demonstrate that reaction kinetics control the results of the experiments.

These results showing disequilibrium among Pt adsorbed and aqueous species are broadly consistent with prior studies, which report possible kinetic effects on Pt behavior (Takahashi et al., 1999; Turner et al., 2006; Cobelo-García et al., 2008). However, our experiments explored substantially longer reaction times than these prior studies and thus demonstrate for the first time the impact of slow reaction kinetics on Pt environmental behavior over multi-month timescales. Such long-term chemical evolution may have been masked in prior work because of how data were reported. For example, studies that only report uptake percentage in adsorption studies (Takahashi et al., 1999; Kubrakova et al., 2011; Maeno et al., 2016; Li et al., 2023) may overlook continued changes in behavior. In the current study, net Pt uptake increases by less than 1% in the chloride-only goethite reactor between 29 and 57 days, but the actual dissolved Pt concentrations are halved with the difference larger than measurement uncertainties (**Fig. 3c**). The persistent disequilibrium of dissolved Pt species and the resulting continued evolution of overall adsorption by iron oxides surfaces renders the results of prior studies unreliable predictors of the environmental behavior of platinum on week to month timescales.

4.2 Effect of pH on Platinum Uptake and Surface Speciation

When Pt is introduced as a Pt-Cl species, increasing pH results in enhanced adsorption to hematite but a negligible impact on adsorption to goethite within 24 hours (**Fig. 2**). Prior studies have also similarly observed that increasing pH enhances Pt adsorption to kaolinite, ferrihydrite, and δ-MnO_2 (Takahashi et al., 1999; Kubrakova et al., 2011; Maeno et al., 2016), although the Pt speciation likely differed in those experiments. A separate study of Pt(II) adsorption to feroxyhyte (Li et al., 2023) found that adsorption was relatively insensitive to pH across the range investigated in this current study, similar to the behavior of goethite. These prior

observations and the current work thus indicate that pH effects on Pt adsorption are mineral-specific.

These variations in the effect of pH on adsorption suggest that surface binding follows mineral-specific reaction stoichiometries. Distinct adsorbed species on goethite and hematite could result in surface complexation reactions of varying pH-dependence through two specific, related mechanisms. Increasing pH results in less positive surface charge for the minerals investigated, which would make the adsorption of a cationic surface species more favorable but would not have an effect on a neutral species. Additionally, differences in proton stoichiometry will result in differing pH dependence of interfacial reactions. A surface complexation model developed for chemically similar Pd(II) involves both such mechanisms and predicts greater adsorption to hematite at higher pH (Wright et al., 2025).

Fitting of the EXAFS spectra clearly indicates that Pt surface reactions differ between hematite and goethite. On hematite, surface Pt undergoes greater hydrolysis at higher pH (**Fig. 5**), consistent with predictions that such aqueous Pt-OH species increase in importance as pH increases (**Fig. 1**). This pH-dependent change in surface speciation indicates that there are multiple surface reactions with different charge- and proton-dependence, resulting in the bulk pH-dependence observed. In contrast, Pt surface coordination on goethite is essentially unchanged across the entire pH range studied, with consistently high numbers of Cl ligands (2.0-2.3; **Table 2**). The pH-insensitivity of this surface Pt indicates that the reaction stoichiometry is substantially different from hematite. Unfortunately, quantitatively assessing the reactions occurring with a surface complexation model is not possible both because of the substantial uncertainty regarding the stability constants of aqueous Pt species (Mountain and Wood, 1988; Wood et al., 1989; Sassani and Shock, 1998; Azaroual et al., 2001, 2003; Byrne, 2003) and

because thermodynamic modeling is not viable for a system that is governed by kinetics. However, the spectroscopic observations of Pt surface speciation indicate mineral-specific variations in adsorption reactions, which in turn result in differences in macroscopic behavior between two chemically-similar iron oxide minerals.

4.3 Slow Ligand Exchange Kinetics Inhibit Platinum Adsorption

In the case of aqueous species with slow ligand exchange, prior work has suggested that the rates of water loss from surface functional groups are the rate-controlling factor for the formation of inner-sphere complexes (Casey et al., 2000). However, this can only apply for species containing bound water or hydroxide. For a fully complexed species such as $Pt(NH_3)_4^{2+}$ or $PtCl_4^{2-}$, inner-sphere adsorption will only occur when a coordinating ligand is lost and/or when a different, less complexed species is formed because it is unlikely that ammonia or chloride can serve as ligand bridges between Pt and Fe for inner-sphere surface complexes. Thus, ligand exchange rates may be an important control on the reactivity of complexed Pt.

While many dissolved metals undergo fast ligand exchange (Lincoln and Merbach, 1995; Richens, 2005), this is not true for Pt, where Pt-Cl species have exchange rates varying from hours to weeks (Martin, 1967; Elding, 1970; Wu et al., 1990) and slow hydrolysis resulting in the formation of polynuclear complexes is known to occur over years (Torapava et al., 2013). In addition, the $Pt(NH_3)_4^{2+}$ complex undergoes ligand exchange on the timespan of decades, with bound ammonia having a mean residence time of 79 years under the experimental conditions of the current study (Brønnum et al., 1992). While these rates vary by many orders of magnitude, they are all slow enough that ligand exchange may have a substantial macroscopic effect on Pt adsorption.

In reactors prepared with the Pt-NH_3 species, no adsorption occurs over several months (**Fig. 3**). This demonstrates that the exceptionally slow ligand exchange of $Pt(NH_3)_4^{2+}$ (Brønnum et al., 1992) prevents it from forming inner-sphere complexes on either mineral or reacting to form a different species. The addition of chloride to systems initially containing Pt-NH_3 species has no observable effect (**Fig. 3**) because Pt-Cl species are likely kinetically or thermodynamically inhibited from forming.

This observation that slow ligand exchange can prevent inner-sphere complexation is indirectly supported by prior work. $Pt(NH_3)_4^{2+}$ has been documented to rapidly form outer-sphere complexes at high pH on amorphous silica and quartz (Schreier and Regalbuto, 2004; Park et al., 2005), but no inner-sphere complexes have been documented. However, iron oxide surfaces will be positively charged across the pH range of weathering zones (Parks, 1965; Thompson and Rodgers, 1977; Fandeur et al., 2009; Ito et al., 2021), making such cationic outer-sphere complexation unfavorable.

Even in cases where initial Pt speciation support faster ligand exchange reactions, Pt may adsorb but continue to evolve in response to changing aqueous speciation. In the chloride-only reactors, the trend of initially rapid adsorption (**Fig. S5**) but continuously changing dissolved Pt concentrations over several months (**Fig. 3**) indicates that equilibrium of adsorbed Pt has not been achieved. The evolution of dissolved Pt aligns well with a transition in reaction rate controls from the faster equilibration of aqueous Pt-Cl species to the slower hydrolysis process (Martin, 1967; Elding, 1970; Wu et al., 1990; Torapava et al., 2013).

Ammonia is predicted to substantially shift Pt speciation under the conditions assessed (**Fig. 1**), which should impact the favorability of adsorption. However, reactors prepared by mixing ammonia with Pt-Cl species are initially indistinguishable from the chloride-only reactors

669 (**Fig. 2,3,S5**), implying that Pt-NH_3 species did not appreciably form within the first few days.
670 Ammonia only begins to induce a macroscopic effect after about a week of aging, suggesting
671 that Pt-NH_3 species form slowly. This is consistent with prior work: H_2O replaces a ligand in
672 $PtCl_4^{2-}$ about an order of magnitude faster than NH_3 (Grantham et al., 1955; Martin, 1967).
673 Except for a single prior study of $Pt(NH_3)_4^{2+}$ (Brønnum et al., 1992), the exchange rates
674 of NH_3 ligands on other relevant Pt(II) species have not been quantitatively documented.
675 However, for at least one Pt-Cl-NH_3 complex, *cis*-$PtCl_2(NH_3)_{2(aq)}$, the Cl ligands are known to
676 exchange on the timespan of hours, while exchange of NH_3 ligands has not been documented
677 (Berners-Price and Appleton, 2000). While it is unclear whether this trend holds universally, the
678 exchange of Cl and H_2O ligands occurring on hours to weeks timescales (Grantham et al., 1955;
679 Elding, 1970; Gröning and Elding, 1989) is orders of magnitude faster than the only quantified
680 NH_3 exchange rate, with a timespan of decades (Brønnum et al., 1992). This observation
681 suggests that for Pt-H_2O-NH_3, Pt-Cl-NH_3, and Pt-H_2O-Cl-NH_3 species, the exchange rate of the
682 more labile ligand(s) may dominate the reactivity of the specific complex with the mineral
683 surface.
684 Slow uptake of adsorbing metals in other systems has been attributed to slow diffusion
685 through nanopores (Axe and Anderson, 1995, 1997; Trivedi and Axe, 1999) or the precipitation
686 of new phases (Scheidegger et al., 1997; Scheidegger et al., 1998; Schlegel and Manceau, 2006;
687 Li et al., 2012). However, the kinetic behavior observed in this study is inconsistent with both of
688 these phenomena. For example, prior work has demonstrated that the dissolved and adsorbed
689 pools of three divalent transition metals take about 5 days to exchange and equilibrate for
690 goethite (Ledingham et al., 2024; Ledingham et al., 2025). This timespan is substantially shorter
691 than the evolution observed in the current study (**Fig. 3**). Additionally, while the neoformation of

a surface phase can result in gradual uptake over the course of more than a month, this also corresponds to an increasing second shell feature in EXAFS spectra from polymerization (Scheidegger et al., 1998; Schlegel and Manceau, 2006). No such shift in the second shell occurs for Pt adsorbed for longer aging times in the current study (**Fig. 4**). Rather, the timescale of different Pt ligand exchange reactions consistently explains the experimental observations, indicating that slow aqueous reactions can macroscopically impact the environmental behavior of Pt.

4.4 Mineral-Specific Evolution of Platinum Surface Speciation and Oxidation State

Platinum surface species observed in this study must derive primarily from aqueous Pt-Cl complexes or subsequent hydrolysis products because of the inert behavior of $Pt(NH_3)_4^{2+}$. While the evolution of aqueous Pt-Cl speciation caused by slow ligand exchange rates can explain gradual changes in adsorption over time (**Fig. 3**), it is unclear whether surface species on hematite and goethite similarly shift over time. The adsorption-desorption dynamics and ligand exchange rates of adsorbed species are uncharacterized for Pt, but established reaction timescales for aqueous Pt-Cl species are similar to the duration of the aging experiments at pH 6 in this study (Elding, 1970; Wu et al., 1990). On both minerals, Pt forms predominately inner-sphere complexes, with about 1 to 2 Cl neighbors after 24 hours of aging at pH 6 (**Tables 1,2**). However, XAS spectra (**Fig. 4,6**) of Pt adsorbed to hematite and goethite for increasing reaction times reveal that Pt surface speciation is highly sensitive to mineralogy.

Known ligand exchange rates and slow hydrolysis behavior suggest that Pt-Cl aqueous species decline in abundance during aging (Elding, 1970; Wu et al., 1990), but this does not correspond to a substantial change in Pt surface speciation on goethite (**Table 2; Fig. 4**). This trend indicates that transient Pt-Cl species are retained by goethite, even as aqueous speciation

continues to evolve. In particular, Pt-Cl species may have a high affinity for goethite, even though they are predicted to decline in abundance with increasing pH (**Fig. 1**). The presence of such species implies that chloride plays a more important role in Pt environmental behavior than previously suggested (e.g., Fuchs and Rose, 1974; Colombo et al., 2008). The stability of Pt-Cl surface species on goethite may be a kinetic phenomenon resulting from inhibited ligand exchange or reflect their energetic stability. The lack of reliable thermodynamic data for aqueous Pt species, potentially a result of long equilibration times caused by slow ligand exchange preventing prior studies of Pt solution thermodynamics from reaching stable conditions, prevents the development of a surface complexation model to further assess the stability of these surface complexes.

In contrast with goethite, adsorbed Pt on hematite undergoes oxidation and hydrolysis over time, with more than 50% of the surface Pt oxidized within 6 days (**Table 3; Fig. 7**). Prior work has demonstrated that Pt adsorbs as square planar Pt(II) species on various iron oxides within 24 hours to 3 days (Koschinsky et al., 2020; Wright et al., 2026). Additionally, a long-term (several months) experiment to elucidate Pt(II) aqueous reaction kinetics did not report the formation of any Pt(IV) species (Elding, 1970). These prior observations suggest that Pt(II) is at least metastable in experiments open to the atmosphere. Based on comparison of the Fe(II)/hematite and Pt(II)/Pt(IV) redox couples, oxidation of Pt(II) by Fe(III) in hematite is not energetically favorable (Stumm and Sulzberger, 1992; Colombo et al., 2008). This suggests that O_2, or a species derived from O_2, serves as the Pt(II) oxidant. Prior work under basic conditions (1 M NaOH) demonstrated that 1 atm O_2 can completely convert dissolved $Pt(OH)_4^{2-}$ to $Pt(OH)_6^{2-}$ within 60 hours (Wu et al., 1990), indicating that oxygen can serve as a Pt oxidant under some conditions. The same study also found that $PtCl(OH)_3^{2-}$ is not completely oxidized

738 by O_2 over the same time period (Wu et al., 1990), demonstrating that Pt(II) speciation affects
739 the rates of oxidation by oxygen. The observation of Pt(II) oxidation only on the hematite
740 surface, and not on goethite, may result from differences in surface catalysis of electron transfer
741 from Pt(II) to O_2 or greater stabilization of Pt(II) surface species on goethite.

742 The oxidation of adsorbed Pt on hematite is unlikely to reflect processes occurring in
743 aqueous solutions. Direct measurement of dissolved Pt oxidation state was not possible due to
744 the low concentrations. However, the solution compositions and dissolved Pt concentrations in
745 the goethite and hematite aging experiments were similar, making it unlikely that distinct
746 aqueous redox pathways occurred in the two systems. For example, if such oxidation occurred in
747 solutions in contact with goethite, observation of increasing Pt(IV) on the goethite surface over
748 time would be expected, similar to hematite. It is possible that, unlike Pt(II), Pt(IV) does not
749 form favorable complexes on goethite, such as has been observed on δ-MnO_2 (Maeno et al.,
750 2016). However, a transition to non-adsorbing Pt(IV) in solution should then result in an increase
751 in dissolved Pt concentrations, the opposite of what is observed (**Fig. 3**).

752 The mineral-specific oxidation of Pt also does not arise from experimental artifacts.
753 Interactions with the X-ray beam during XAS measurements did not induce Pt oxidation.
754 Samples were measured at 78 K to hinder migration of beam-induced radicals, multiple scans
755 collected for each sample showed no evidence of redox changes in the X-ray beam, and prior
756 measurements for the chemically-similar Pd(II) observed it undergoes reduction, not oxidation,
757 upon exposure to intense X-ray beams at ambient temperature (Wright et al., 2025).
758 Additionally, the aging experiments were conducted in foil-wrapped bottles and tubes to prevent
759 light exposure that could cause photo-oxidation.

Mineral-driven oxidation of Pt has been previously demonstrated to occur on manganese oxides (Maeno et al., 2016; Koschinsky et al., 2020) and Pt(IV) associated with such minerals is the dominant form of Pt in marine ferromanganese deposits (Kashiwabara et al., 2026; Liao et al., 2026). However, prior evidence for Pt oxidation on iron oxides is mixed (Koschinsky et al., 2020; Li et al., 2023). The current study demonstrates that such oxidation can occur on hematite, but it is either kinetically or thermodynamically inhibited from occurring on goethite. A surface-mediated oxidation process potentially enables a larger variety of minerals to drive Pt oxidation in the environment since the mineral is not the oxidant. However, such a process might be highly sensitive to the speciation of adsorbed Pt, as is suggested by the current work. As such a process occurs on days to months timescales (**Fig. 7**) with no apparent change in macroscopic behavior (**Fig. 3**), prior studies over short timescales (a few days) and with no spectroscopic measurements may fail to detect this process and thus not accurately predict Pt environmental behavior. For both iron oxide minerals studied, the additional presence of ammonia had no substantive effect on the Pt surface speciation nor the trend in oxidation state over time (**Fig. 4-7**). However, ammonia does inhibit adsorption over several months in reactors prepared with the Pt-Cl species (**Fig. 3**). The slow formation of an aqueous Pt complex with at least one NH_3 ligand can explain the macroscopic results, but this species does not appear to appreciably affect Pt surface speciation within 2 months of aging.

4.5 Implications for platinum behavior in terrestrial weathering zones

The experimental dataset reveals that Pt adsorption evolves over days to months in response to slow aqueous Pt reactions as well as surface-mediated oxidation in systems containing hematite. While the slow ligand exchange rates for many Pt species have been well known for decades (e.g., Elding, 1970), the present study clearly demonstrates that the reaction

kinetics of dissolved Pt control its retention by mineral surfaces on substantially longer timescales than for other metals. These findings are distinct from aging effects observed for divalent first-row transition metals like Ni(II) and Zn(II), which result from structural incorporation (Ledingham et al., 2024; Ledingham et al., 2025) or neoformation of new phases (Scheidegger et al., 1997; Scheidegger et al., 1998; Schlegel and Manceau, 2006; Li et al., 2012). Rather, slow ligand exchange in solution has macroscopic effects on Pt retention in the environment associated with either stable surface speciation (goethite) or surface-mediated oxidation (hematite).

Prior reactive transport modeling focused on Ni mineralization during laterite formation has generally treated aqueous and adsorption reactions as equilibrated, but considered kinetic controls on dissolution and precipitation (Domènech et al., 2017; Myagkiy et al., 2017; Myagkiy et al., 2019). However, if chemical reaction rates, including aqueous complexation, are slower than transport rates then there will be persistent local geochemical disequilibrium (Molins et al., 2012; Molins and Knabner, 2019). A prior reactive transport model for the formation of a laterite resulted in a calculated water residence time of 2.7 years (Domènech et al., 2017), far shorter than ligand exchange of $Pt(NH_3)_4^{2+}$ (Brønnum et al., 1992) or long-term hydrolysis (Torapava et al., 2013). Differences between laterites in the water infiltration rate, porosity, and other factors that impact water flow may result in shorter or longer residence times that will influence the degree of Pt retention.

Additionally, modeling of fluid flow at the pore scale often results in predictions of highly spatially heterogeneous behavior (e.g., Molins et al., 2012; Molins and Knabner, 2019), particularly in unsaturated zones (e.g., Jiménez-Martínez et al., 2015). These potential grain-scale variations in residence time will drive local variability in Pt uptake. For example, aqueous

Pt speciation might continue to evolve as fluid flows through the subsurface, but the amount of Pt adsorbed would substantially vary along the path. The sensitivity of Pt surface speciation to residence time will also be controlled by the relative abundance of hematite versus goethite.

Furthermore, the pH of weathering profiles typically increases with depth (e.g., Thompson and Rodgers, 1977; Fandeur et al., 2009; Ito et al., 2021), which may additionally influence Pt behavior. Increasing pH results in moderately enhanced Pt adsorption to hematite, increasing by a factor of ~2 from pH 4 to 8 (**Fig. 2**). However, no such trend is observed for goethite (**Fig. 2**). Thus, pH- and depth-dependent Pt retention trends will vary across different weathering zones, influenced by iron oxide mineralogy. Acidic conditions in the upper regions of hematite-rich weathering profiles, as well as microenvironments produced from weathering of sulfide grains (e.g., Dockrey et al., 2014), may promote weak leaching of Pt, which will then be better retained at depth where the pH rises. However, such spatial trends are not predicted to occur in goethite-dominated laterites.

A previously developed model for Pt-Pd fractionation in weathering zones attributed such fractionation as being driven by iron oxide mineralogy (Wright et al., 2026), which is in turn influenced by climate (Schwertmann, 1971; Kämpf and Schwertmann, 1983; Hyland et al., 2015; Long et al., 2016). While this model addresses weakly acidic conditions (pH 4), the new dataset confirms that mineralogical preference in Pt binding occurs even at higher pH. Fractionation will occur in hematite-rich zones due to preferential retention of Pt, contingent on Pd adsorption to hematite increasing with pH, as has been suggested by prior work (Wright et al., 2025).

The mineral surfaces present will also influence the redox speciation of Pt in weathering profiles. Platinum(II) slowly oxidizes to Pt(IV) on the surface of hematite, but the same process does not occur on goethite (**Fig. 7**). While the exact molecular-scale process that results in

oxidation is uncertain, Pt oxidation is likely mediated by the hematite surface (**Section 4.4**). Thus, over time, surface-promoted oxidation of Pt and exchange with solution will gradually result in a transition to Pt(IV) in hematite-rich weathering zones. In contrast, the results of this study indicate that Pt(II) will persist in goethite-rich laterites.

The transition to Pt(IV) in hematite-dominated environments has additional implications for the reactivity of Pt. While there is little data on Pt(IV) aqueous reactions or ligand exchange kinetics, it is generally more kinetically inhibited than Pt(II) (Johnson et al., 1962; Elding and Gustafson, 1977; Gröning and Elding, 1989; Richens, 1997). For example no detectable water exchange for $[Pt(H_2O)_5Cl]^{3+}$ was measured within 12 hours using ^{195}Pt NMR (Gröning and Elding, 1989). While Pt(II) reactions are already quite slow, the transition to Pt(IV) in hematite-rich zones might result in even greater kinetically-controlled behavior.

Finally, mineralization of organic matter in soils and shallow sections of weathering zones produces ammonia that could bind to available Pt. Such environments that contain abundant ammonia will further promote the mobilization of Pt through the formation of highly mobile aqueous Pt-NH_3 species. However, the formation of Pt-NH_3 species is likely slow. Thus, as fluid flows through the subsurface, substantial amounts of Pt may be removed from solution via adsorption before Pt-Cl and Pt-OH species convert to Pt-NH_3 complexes. Once formed, Pt-NH_3 species will be highly mobile because they are not retained by most mineral surfaces. The presence of such species in the weathering zone will also promote the desorption of Pt surface species.

The kinetic inertness of ammine groups may also result in these Pt-NH_3 species readily persisting even when no longer thermodynamically favored. The exceptionally slow ligand exchange of $Pt(NH_3)_4^{2+}$ (Brønnum et al., 1992) suggests that weathering zones are in

disequilibrium with respect to Pt-NH_3 species. Outer-sphere complexation, which may retain such species, will only occur at high pH when at least some mineral surfaces are sufficiently negatively charged. However, cation exchange into clay layers may provide an alternative retention mechanism in some geochemical environments, but the reactivity of Pt-NH_3 aqueous complexes with clay minerals has not been studied to date.

5. CONCLUSION

The fate of Pt in terrestrial weathering zones is controlled by a complicated interplay of iron oxide mineralogy, complexing ligands, and the kinetic of aqueous complexation and surface-mediated oxidation. The slow formation of Pt-NH_3 species in the environment creates a highly mobile pool of Pt that is not readily retained by mineral surfaces due to inert ligand exchange rates. Once formed, the mobility of Pt-NH_3 species likely extends to conditions where they are no longer thermodynamically favored because they require decades to dissociate in solution. In contrast, Pt-Cl species rapidly adsorb as corner-sharing species on both hematite and goethite. However, adsorption continues to evolve over several months, likely reflecting changes in Pt solution speciation due to ongoing aqueous reactions. In the absence of ammonia, the gradual enhancement of adsorption likely reflects a conversion from Pt-Cl species to Pt-OH species in solution, but results in diverging surface speciation on hematite versus goethite. Increasing reaction times result in hydrolysis and oxidation of Pt on the hematite surface. In contrast, no such transformation or oxidation occurs on the goethite surface. The speciation and amount of retained Pt in weathering zones will be kinetically controlled, reflecting spatial heterogeneity in fluid residence time at the pore scale. A complete conversion from Pt(II) to Pt(IV) in hematite-rich weathering zones may further inhibit Pt ligand exchange kinetics.

Platinum mobility and retention in laterites and other weathering environments reflects chemical reaction rates that occur on similar or longer timescales compared to water residence times.

Data Availability

Data are available through Mendeley Data at https://doi.org/10.17632/9bhtr2w54w.1.

Acknowledgments

This material is based upon work supported by the U.S. Department of Energy, Office of Science, Office of Basic Energy Sciences, Geosciences program under Award Number DE-SC0022213. The contribution of E.G.W. was supported by a National Science Foundation Graduate Research Fellowship under Grant No. DGE-2139839. Any opinions, findings, and conclusions or recommendations expressed in this material are those of the author and do not necessarily reflect the views of the National Science Foundation. This research used beamline 6-BM of the National Synchrotron Light Source II, a US Department of Energy Office of Science User Facility operated for the Department of Energy Office of Science by Brookhaven National Laboratory under contract no. DE-SC0012704. We thank beamline scientist Bruce Ravel for his assistance with data collection and for measuring the platinum(II) acetylacetonate standard. The authors acknowledge the support of the Chemical and Environmental Analysis Facility (CEAF) at Washington University in St. Louis for providing access to BET analysis. The authors thank Xuewen Wang, Bob Anleitner, and Paul Carpenter for assistance with analytical instruments and data collection.

Appendix A. Supplementary Material

The Supplementary Material contains additional information about mineral batches used in experiments, thermodynamic modeling, and EXAFS fitting of standards. Results from a preliminary experiment investigating the effect of ammonia at pH 7 are presented. Data from the shorter-term kinetic experiment and mineral-free controls, as well as trends in the XAS data, are visualized.

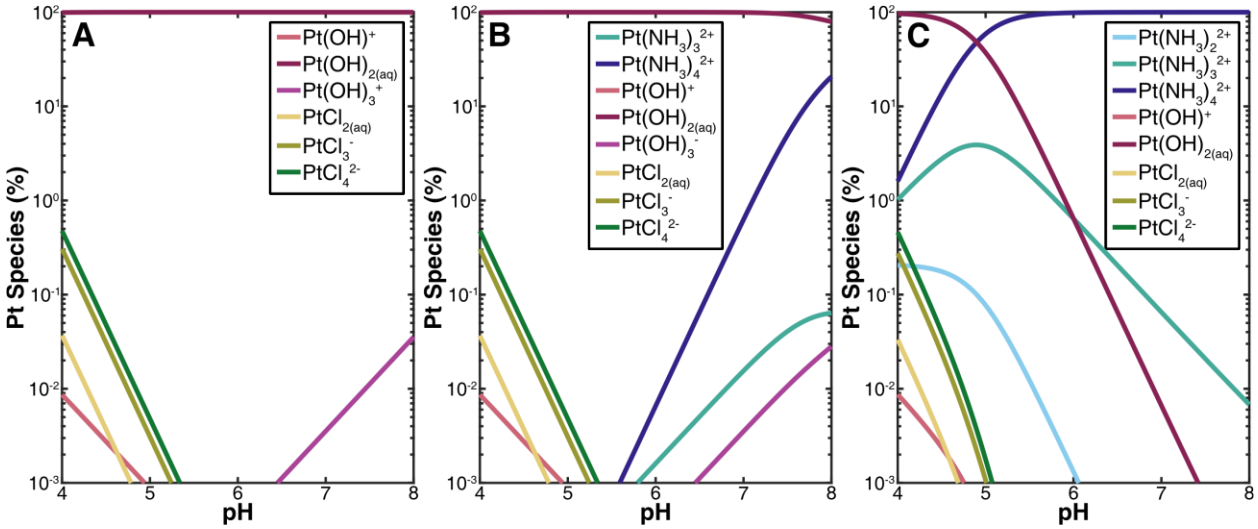

Figure 1. The relative abundances of Pt(II) species from pH 4 to 8 in the presence of (**A**) 10 mM chloride, (**B**) 10 mM chloride and 0.25 mM ammonia, and (**C**) 10 mM chloride and 10 mM ammonia. Species concentrations were calculated using the equilibrium constants provided by Mountain and Wood (1988) and Wood et al. (1989). Species that represent less than 0.001% of the total Pt are not shown. Note that the use of a different thermodynamic dataset will result in predictions of the relative abundance of Pt-OH and Pt-Cl species that differ by up to six orders of magnitude (Wright et al., 2026).

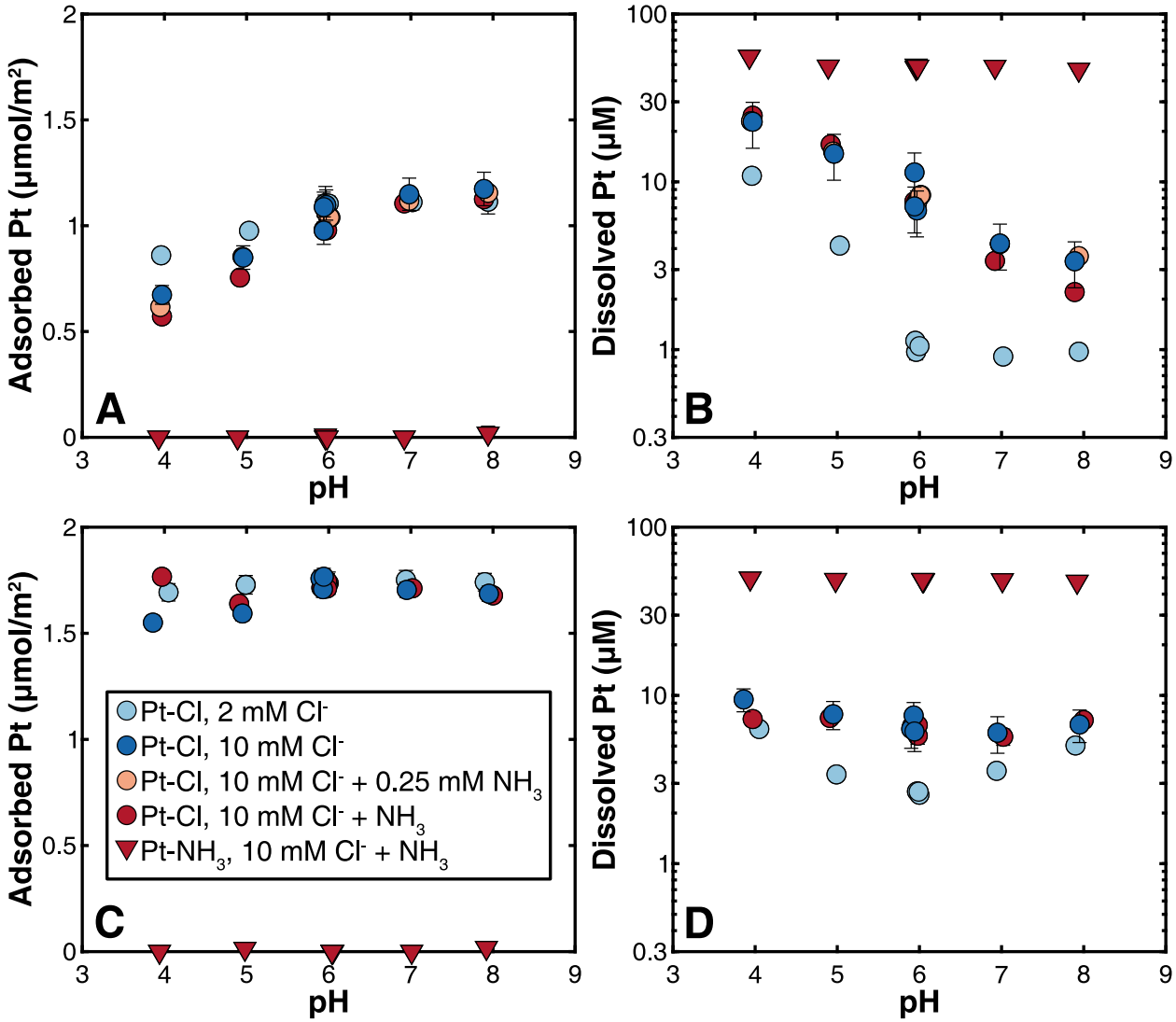

Figure 2. Platinum adsorption (**A,C**) and remaining dissolved Pt (**B,D**) as a function of pH to hematite (**A,B**) and goethite (**C,D**) after a reaction time of 24 hours in different solution compositions and prepared with different Pt stock solutions. Errors smaller than the symbols are not shown.

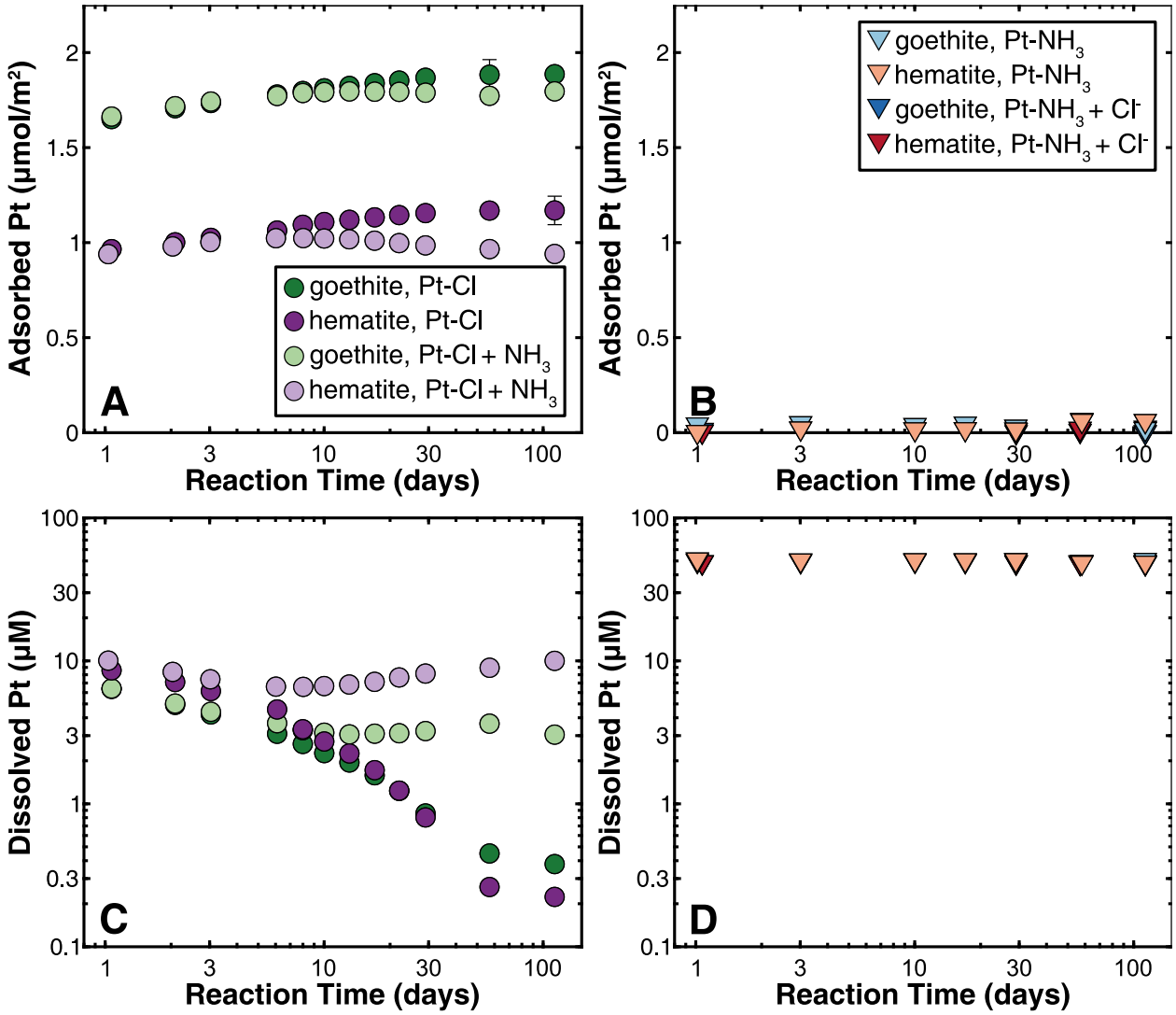

Figure 3. Platinum adsorption to hematite and goethite (**A,B**) at pH 6.0±0.2, and the corresponding remaining dissolved Pt concentrations (**C**,**D**), as a function of reaction time in the longer-term kinetic reactors. Reactors were prepared with Pt-Cl complexes (**A,C**) or Pt-NH_3 complexes (**B,D**). Errors smaller than the symbols are not shown. All reactors contained 10 mM chloride; 10 mM chloride and 10 mM ammonia; or 10 mM ammonia.

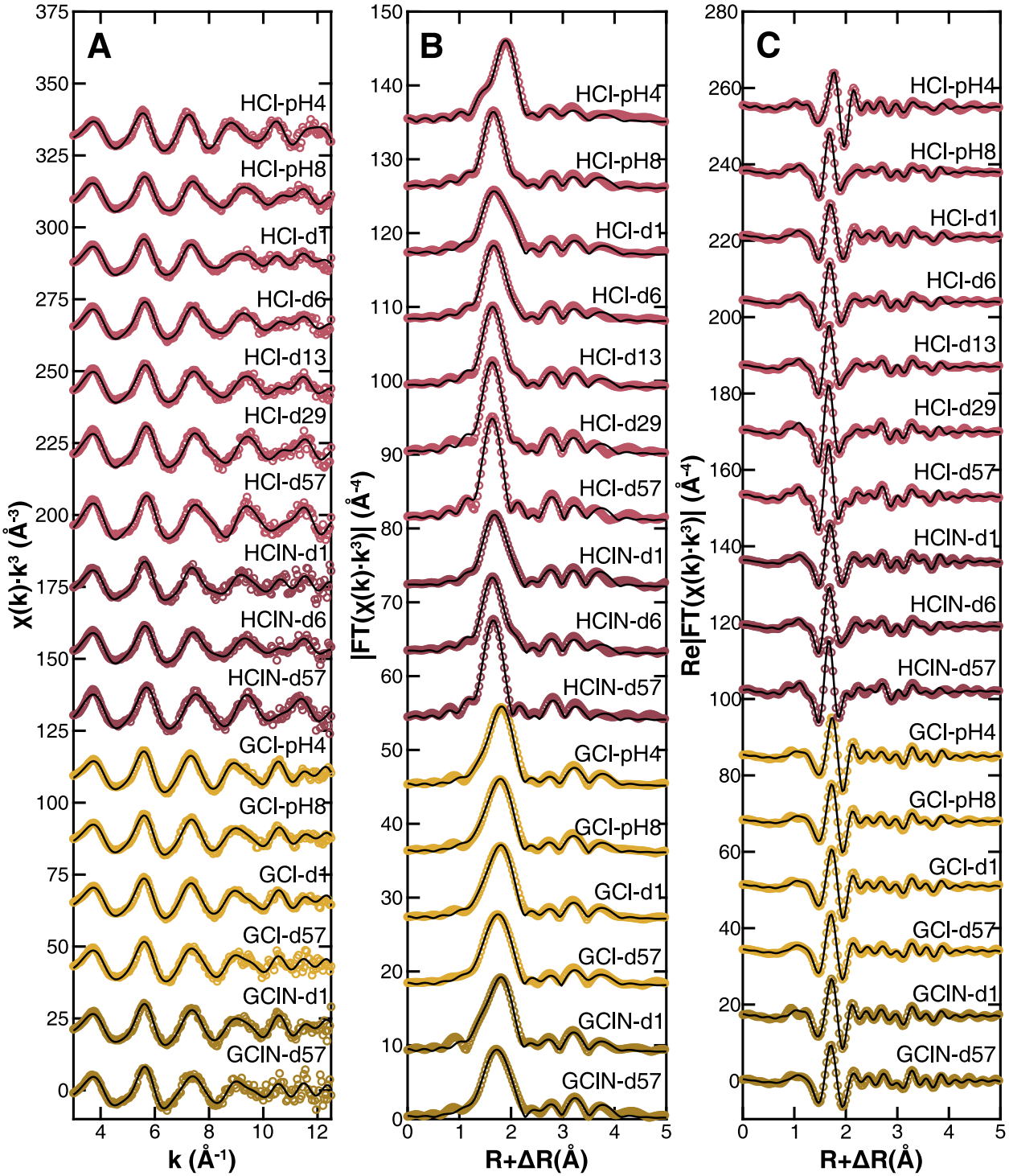

Figure 4. Data (symbols) and structural model fit (solid black line) to the (**A**) Pt L_3-edge EXAFS spectra, (**B**) Fourier transform magnitudes, and (**C**) real components of the Fourier transforms. Detailed sample information is provided in **Tables 1, 2,** and **S2**.

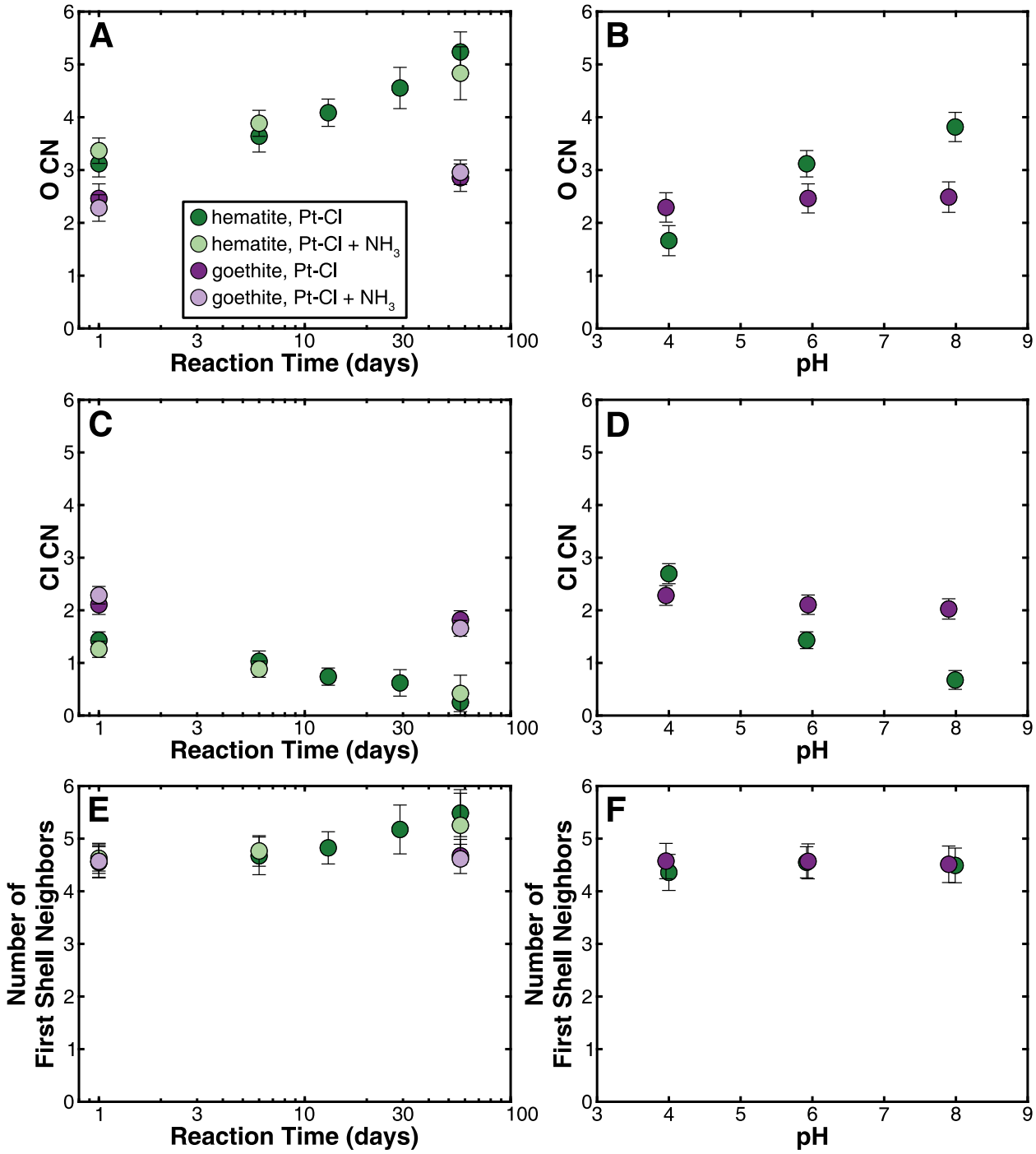

Figure 5. Summary of the variations in changes in the O coordination number (CN; **A,B**), Cl CN (**C,D**), and total number of first shell neighbors (**E,F**) for Pt surface species as a function of reaction time at pH 6 (**A,C,E**) or changing pH with 24 hour reaction times (**B,D,F**). All parameters (**Tables 1,2**) are derived from fits to the EXAFS spectra of solid-associated Pt (**Fig. 4**).

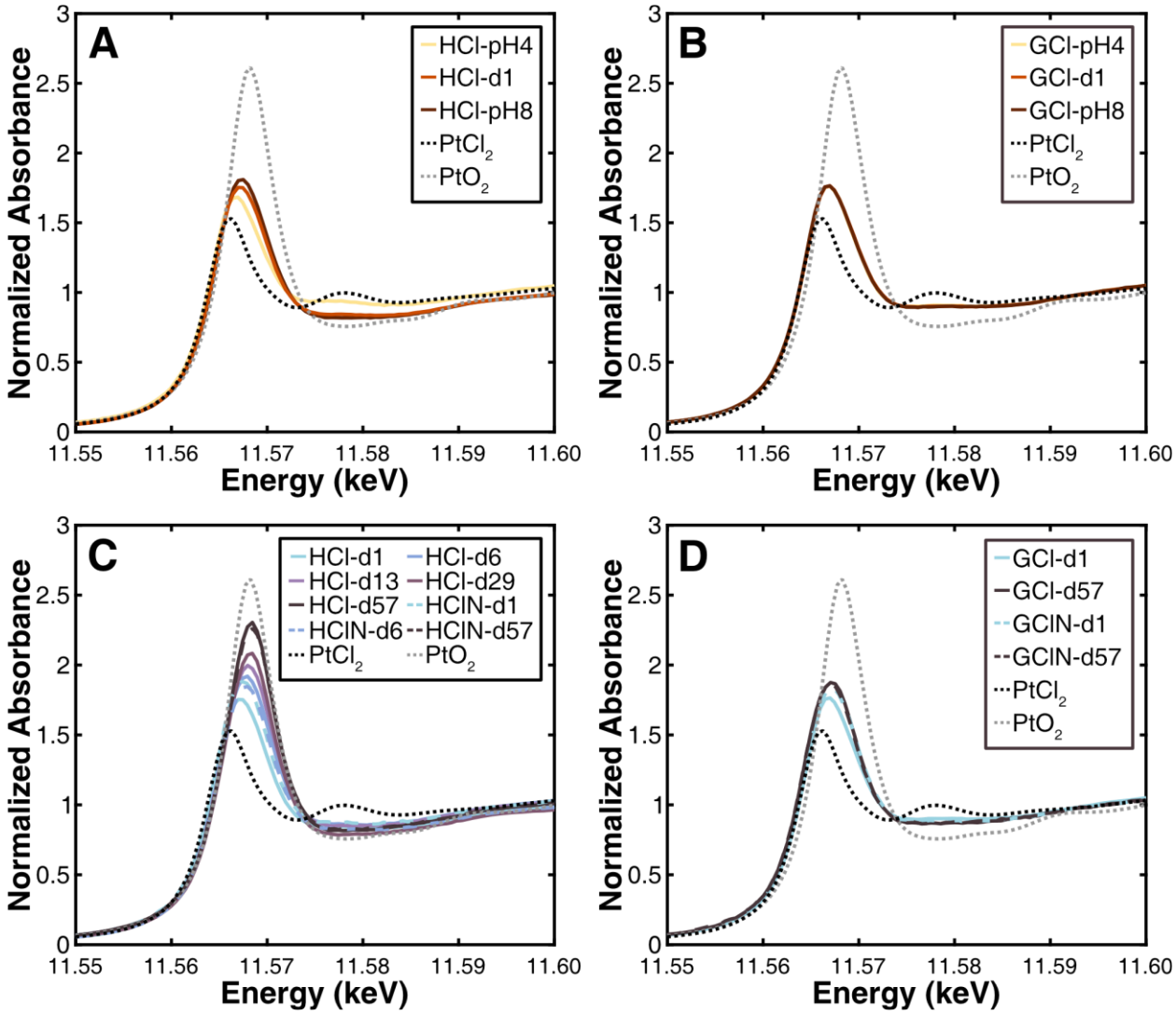

Figure 6. Pt L_3-edge XANES spectra of hematite (**A,C**) and goethite (**B,D**) samples as a function of pH after 24 hours of reaction (**A,B**) and variable reaction time at pH 6.0±0.2 (**C,D**). Detailed sample information is provided in **Tables 1, 2,** and **S2**. Spectra of $Pt^{II}Cl_2$ and $Pt^{IV}O_2$ are shown for reference.

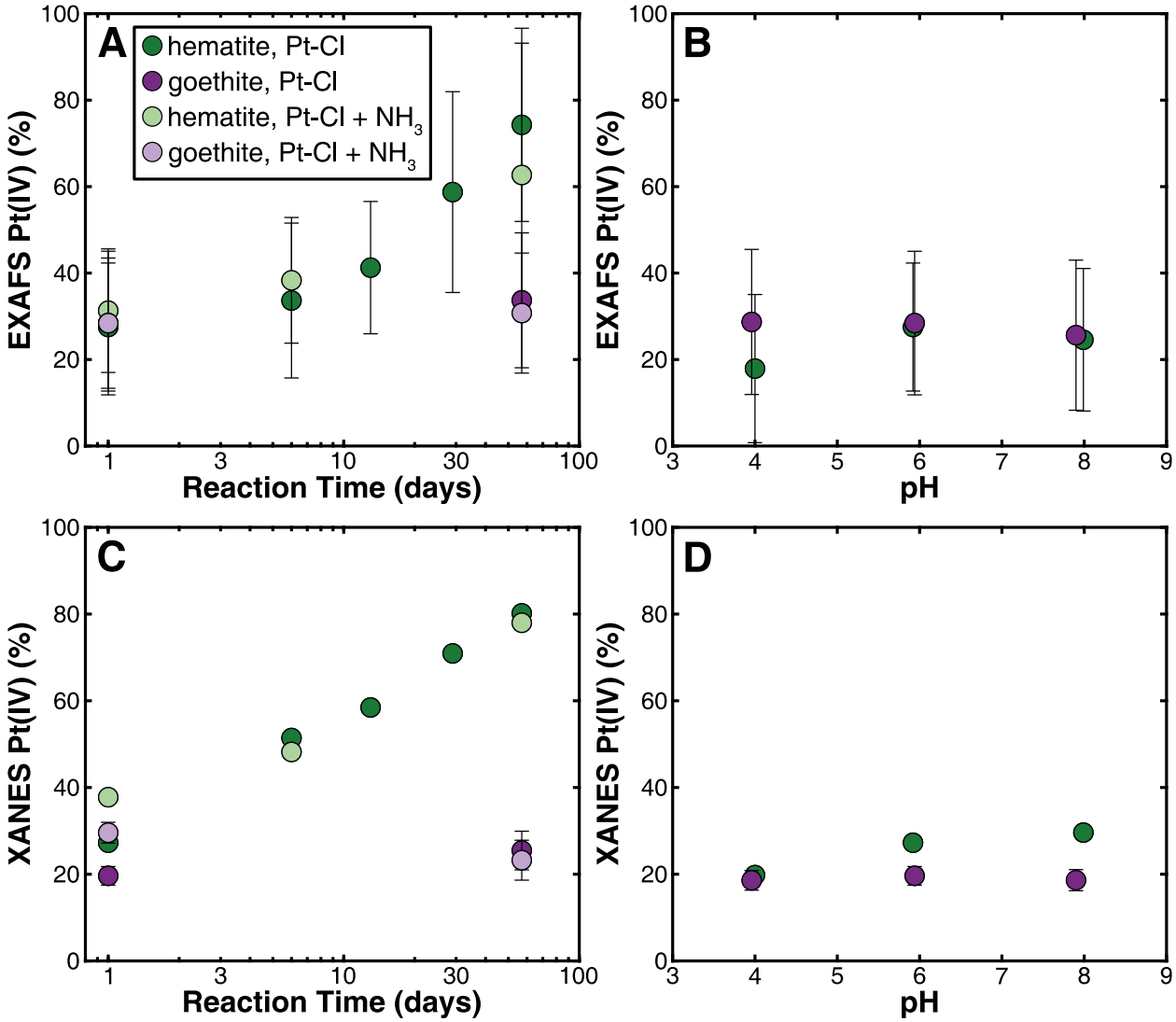

Figure 7. Summary of changes in Pt oxidation state with increasing reaction time (**A,C**) and pH (**B,D**). The oxidation state (as percent Pt(IV)) calculated from the EXAFS-obtained sum of first shell paths (**Tables 1,2**) is shown as a function of reaction time (**A**) or pH (**B**). The oxidation state calculated from linear combination fits of the XANES region (see **Table 3**) is shown as a function of reaction time (**C**) or pH (**D**). Errors smaller than the symbols not shown.

948 **Table 1.** Platinum L_3-edge EXAFS fitting parameters for hematite samples.

Sample[a]	Reaction Time (days)	Target NH_3 (mM)	Path	CN[b]	R (Å)[c]	σ^2 (Å^2)[d]	ΔE_0 (eV)[e]	*R* factor[f]	χ_v^{2f}
HCl-pH4	1	0	Pt-O	1.7(3)[g]	2.01(2)	0.0026	12(2)	0.024	6.17
			Pt-Cl	2.7(2)	2.29(1)	0.0026			
			Pt-Fe1	0.5(3)	3.04(4)	0.005			
			Pt-Fe2	2.5(8)	3.71(2)	0.005			
			Pt-Fe3	3(1)	3.90(2)	0.005			
HCl-pH8	1	0	Pt-O	3.8(3)	2.01(1)	0.0026	12(1)	0.019	12.55
			Pt-Cl	0.7(2)	2.27(2)	0.0026			
			Pt-Fe1	0.5(2)	3.08(3)	0.005			
			Pt-Fe2	2.2(7)	3.69(2)	0.005			
			Pt-Fe3	2.8(8)	3.87(2)	0.005			
HCl-d1	1	0	Pt-O	3.1(2)	2.01(1)	0.0026	12(1)	0.023	17.43
			Pt-Cl	1.4(2)	2.28(1)	0.0026			
			Pt-Fe1	0.5(3)	3.08(3)	0.005			
			Pt-Fe2	2.8(7)	3.72(2)	0.005			
			Pt-Fe3	2.9(8)	3.90(2)	0.005			
HCl-d6	6	0	Pt-O	3.6(3)	2.01(1)	0.0026	12(2)	0.022	6.99
			Pt-Cl	1.0(2)	2.27(2)	0.0026			
			Pt-Fe1	0.7(3)	3.08(2)	0.005			
			Pt-Fe2	2.4(8)	3.69(2)	0.005			
			Pt-Fe3	2.7(9)	3.87(2)	0.005			
HCl-d13	13	0	Pt-O	4.1(3)	2.003(9)	0.0026	12(1)	0.018	9.24
			Pt-Cl	0.7(2)	2.27(2)	0.0026			
			Pt-Fe1	0.7(3)	3.08(2)	0.005			
			Pt-Fe2	2.6(7)	3.70(2)	0.005			
			Pt-Fe3	2.7(8)	3.88(2)	0.005			
HCl-d29	29	0	Pt-O	4.6(4)	2.00(1)	0.0026	11(2)	0.026	9.99
			Pt-Cl	0.6(3)	2.25(3)	0.0026			
			Pt-Fe1	1.0(3)	3.07(2)	0.005			
			Pt-Fe2	2.9(9)	3.66(2)	0.005			
			Pt-Fe3	3(1)	3.84(2)	0.005			
HCl-d57	57	0	Pt-O	5.2(4)	2.00(1)	0.0026	13(2)	0.030	15.02
			Pt-Cl	0.3(2)	2.28(7)	0.0026			
			Pt-Fe1	1.2(4)	3.09(2)	0.005			
			Pt-Fe2	3(1)	3.67(3)	0.005			
			Pt-Fe3	3(1)	3.84(3)	0.005			
HClN-d1	1	10	Pt-O	3.4(2)	2.007(9)	0.0026	11(1)	0.014	2.86
			Pt-Cl	1.3(2)	2.27(1)	0.0026			
			Pt-Fe1	0.8(2)	3.09(2)	0.005			
			Pt-Fe2	3.5(6)	3.68(1)	0.005			
			Pt-Fe3	4.1(7)	3.86(1)	0.005			
HClN-d6	6	10	Pt-O	3.9(2)	2.005(9)	0.0026	12(1)	0.020	10.81
			Pt-Cl	0.9(2)	2.28(2)	0.0026			
			Pt-Fe1	0.6(3)	3.09(3)	0.005			
			Pt-Fe2	2.6(7)	3.69(2)	0.005			
			Pt-Fe3	2.7(8)	3.86(2)	0.005			
HClN_d57	57	10	Pt-O	4.8(5)	2.01(1)	0.0026	13(2)	0.024	7.47
			Pt-Cl	0.4(3)	2.23(4)	0.0026			
			Pt-Fe1	0.9(3)	3.09(2)	0.005			
			Pt-Fe2	2(1)	3.69(3)	0.005			
			Pt-Fe3	2(1)	3.87(4)	0.005			

[a]See **Table S2** for more details regarding individual samples. HCl-pH4 was previously published (Wright et al., 2026) but has been refit. All samples were pH 6.0±0.2 except for HCl-pH4 and HCl-pH8.
[b]Coordination number.
[c]Interatomic distance.
[d]Debye-Waller factor.
[e]Energy shift parameter.
[f]Goodness-of-fit parameters (Kelly et al., 2008).
[g]The estimated standard deviations as errors in the last digit are given in parentheses. Constrained parameters are listed with no uncertainties.

Table 2. Platinum L_3-edge EXAFS fitting parameters for goethite samples.

Sample[a]	Reaction Time (days)	Target NH_3 (mM)	Path	CN[b]	R (Å)[c]	σ^2 (Å^2)[d]	ΔE_0 (eV)[e]	*R* factor[f]	χ_v^{2f}
GCl-pH4	1	0	Pt-O	2.3(3)[g]	2.01(2)	0.0026	11(1)	0.013	14.81
			Pt-Cl	2.3(2)	2.269(9)	0.0026			
			Pt-Fe1	0.3(2)	3.08(4)	0.005			
			Pt-Fe2	3.6(6)	3.69(1)	0.005			
			Pt-Fe3	3.5(7)	3.89(1)	0.005			
GCl-pH8	1	0	Pt-O	2.5(3)	2.01(2)	0.0026	11(2)	0.017	14.09
			Pt-Cl	2.0(2)	2.27(1)	0.0026			
			Pt-Fe1	0.4(2)	3.06(4)	0.005			
			Pt-Fe2	3.3(7)	3.68(1)	0.005			
			Pt-Fe3	3.1(8)	3.87(2)	0.005			
GCl-d1	1	0	Pt-O	2.5(3)	2.01(1)	0.0026	11(2)	0.016	22.86
			Pt-Cl	2.1(2)	2.27(1)	0.0026			
			Pt-Fe1	0.4(2)	3.08(4)	0.005			
			Pt-Fe2	3.2(7)	3.69(1)	0.005			
			Pt-Fe3	3.2(8)	3.88(2)	0.005			
GCl-d57	6	0	Pt-O	2.9(3)	2.00(1)	0.0026	11(1)	0.016	4.45
			Pt-Cl	1.8(2)	2.27(1)	0.0026			
			Pt-Fe1	0.5(3)	3.12(3)	0.005			
			Pt-Fe2	2.9(7)	3.69(1)	0.005			
			Pt-Fe3	2.9(8)	3.89(2)	0.005			
GClN-d1	1	10	Pt-O	2.3(3)	1.98(1)	0.0026	9(1)	0.016	7.51
			Pt-Cl	2.3(2)	2.251(9)	0.0026			
			Pt-Fe1	0.6(2)	3.07(3)	0.005			
			Pt-Fe2	3.8(7)	3.67(1)	0.005			
			Pt-Fe3	3.3(8)	3.87(2)	0.005			
GClN-d57	57	10	Pt-O	3.0(2)	2.00(1)	0.0026	11(1)	0.014	3.02
			Pt-Cl	1.7(2)	2.272(9)	0.0026			
			Pt-Fe1	0.8(2)	3.14(2)	0.005			
			Pt-Fe2	4.1(6)	3.68(1)	0.005			
			Pt-Fe3	3.9(7)	3.88(1)	0.005			

[a]See **Table S2** for more details regarding individual samples. GCl-pH4 was previously published (Wright et al., 2026) but has been refit. All samples were pH 6.0±0.2 except for GCl-pH4 and GCl-pH8.

[b]Coordination number.

[c]Interatomic distance.

[d]Debye-Waller factor.

[e]Energy shift parameter.

[f]Goodness-of-fit parameters (Kelly et al., 2008).

[g]The estimated standard deviations as errors in the last digit are given in parentheses. Constrained parameters are listed with no uncertainties.

Table 3. Results of linear combination fitting of XANES spectra.

Sample[a]	Pt(II)-O[b]	Pt(II)-Cl[b]	Pt(IV)-O[b]	Sum	R factor	χ_v^2	Pt(II) (%)	Pt(IV) (%)
GCl-pH4	0.27(6)[c]	0.55(4)	0.19(2)	1.01(8)	0.0027	0.0593	81(7)	19(2)
GCl-pH8	0.29(7)	0.54(4)	0.19(2)	1.01(8)	0.0032	0.0682	81(8)	19(2)
GCl-d1	0.27(6)	0.55(4)	0.20(2)	1.01(7)	0.0025	0.0524	80(7)	20(2)
GCl-d57	0.4(1)	0.41(8)	0.26(5)	1.0(2)	0.0117	0.2354	70(10)	25(4)
GClN-d1	0.22(7)	0.50(4)	0.30(2)	1.01(8)	0.0035	0.0670	70(8)	30(2)
GClN-d57	0.4(1)	0.41(8)	0.24(5)	1.0(2)	0.0127	0.2519	80(10)	23(5)
HCl-pH4	0.06(4)	0.75(3)	0.20(1)	1.01(5)	0.0012	0.0238	80(5)	20(1)
HCl-pH8	0.38(4)	0.30(2)	0.29(1)	0.97(5)	0.0009	0.0211	70(5)	30(1)
HCl-d1	0.29(4)	0.42(2)	0.27(1)	0.97(5)	0.0010	0.0216	73(5)	27(1)
HCl-d6	—[d]	0.485(5)	0.514(5)	1.000(7)	0.0014	0.0295	48.6(5)	51.4(5)
HCl-d13	—	0.415(7)	0.584(6)	1.00(1)	0.0025	0.0567	41.5(7)	58.5(6)
HCl-d29	—	0.281(8)	0.684(7)	0.97(1)	0.0027	0.0635	29.1(8)	70.9(7)
HCl-d57	—	0.199(9)	0.804(8)	1.00(1)	0.0036	0.0999	19.8(9)	80.2(8)
HClN-d1	0.18(4)	0.44(2)	0.38(1)	1.01(5)	0.0010	0.0211	62(4)	38(1)
HClN-d6	0.07(4)	0.43(3)	0.47(1)	0.97(5)	0.0013	0.0254	52(5)	48(2)
HClN-d57	—	0.22(1)	0.78(1)	1.00(1)	0.0051	0.1364	22(1)	78(1)

[a]See **Table S2** for more details regarding individual samples. GCl-pH4 and HCl-pH4 were previously published (Wright et al., 2026).

[b]The standards used were platinum(II) acetylacetonate for Pt(II)-O, ammonium tetrachloroplatinate for Pt(II)-Cl, and platinum(IV) oxide for Pt(IV)-O.

[c]Uncertainties in the last digit are given in parentheses.

[d]Components that resulted in weights that were negative or within error of 0 were excluded from the final fit.

REFERENCES

Ahokpossi D.P., Atangana A. and Vermeulen P.D. (2018) Hydro-geochemical characterizations of a platinum group element groundwater system in Africa. *J. Afr. Earth Sci.* **138**, 348-366.

Aiglsperger T., Proenza J.A., Zaccarini F., Lewis J.F., Garuti G., Labrador M. and Longo F. (2015) Platinum group minerals (PGM) in the Falcondo Ni-laterite deposit, Loma Caribe peridotite (Dominican Republic). *Miner. Deposita* **50**, 105-123.

Alexander A., Ndambuki J., Salim R. and Manda A. (2017) Assessment of Spatial Variation of Groundwater Quality in a Mining Basin. *Sustainability* **9**, 823.

Ankudinov A.L., Ravel B., Rehr J.J. and Conradson S.D. (1998) Real-space multiple-scattering calculation and interpretation of x-ray-absorption near-edge structure. *Phys. Rev. B* **58**, 7565-7576.

Arpalahti J., Sillanpää R. and Mikola M. (1994) Facile Isolation and Crystal Structure Determination of *trans*-[$PtCl(OH)(NH_3)_2$]·H_2O. *J. Chem. Soc., Dalton Trans.* **9**, 1499-1500.

Atoji M., Richardson J.W. and Rundle R.E. (1957) On the Crystal Structures of the Magnus Salts, $Pt(NH_3)_4PtCl_4$. *J. Am. Chem. Soc.* **79**, 3017-3020.

Axe L. and Anderson P.R. (1995) Sr Diffusion and Reaction with Fe Oxides: Evaluation of the Rate-Limiting Mechanism for Sorption. *J. Colloid Interface Sci.* **175**, 157-165.

Axe L. and Anderson P.R. (1997) Experimental and Theoretical Diffusivities of Cd and Sr in Hydrous Ferric Oxide. *J. Colloid Interface Sci.* **185**, 436-448.

Azaroual M., Romand B., Freyssinet P. and Disnar J.-R. (2001) Solubility of platinum in aqueous solutions at 25°C and pHs 4 to 10 under oxidizing conditions. *Geochim. Cosmochim. Acta* **65**, 4453-4466.

Azaroual M., Romand B., Freyssinet P. and Disnar J.-R. (2003) Response to the comment by R. H. Byrne on "Solubility of platinum in aqueous solutions at 25°C and pHs 4 to 10 under oxidizing conditions" (2001) Geochim. Cosmochim. Acta 65, 4453–4466. *Geochim. Cosmochim. Acta* **67**, 2511-2513.

Baas Becking L.G.M., Kaplan I.R. and Moore D. (1960) Limits of the Natural Environment in Terms of pH and Oxidation-Reduction Potentials. *J. Geol.* **68**, 243-284.

Becker M., Wiese J. and Ramonotsi M. (2014) Investigation into the mineralogy and flotation performance of oxidised PGM ore. *Miner. Eng.* **65**, 24-32.

Berners-Price S.J. and Appleton T.G. (2000) The Chemistry of Cisplatin in Aqueous Solution. In *Platinum-Based Drugs in Cancer Therapy* (eds. L. R. Kelland and N. P. Farrell). Humana Press, Totowa, NJ. pp. 3-35.

Brønnum B., Johansen H.S. and Skibsted L.H. (1992) Ammine Ligand Exchange in Tetraammineplatinum(II) in Aqueous Solution. *Inorg. Chem.* **31**, 3023-3025.

Brown G.E., Foster A.L. and Ostergren J.D. (1999) Mineral surfaces and bioavailability of heavy metals: A molecular-scale perspective. *Proc. Natl. Acad. Sci. USA* **96**, 3388-3395.

Byrne R.H. (2003) Comment on "Solubility of platinum in aqueous solutions at 25°C and phs 4 to 10 under oxidizing conditions" by Mohamed Azaroual, Bruno Romand, Philippe Freyssinet, and Jean-Robert Disnar. *Geochim. Cosmochim. Acta* **67**, 2511-2513.

Casey W.H., Phillips B.L., Karlsson M., Nordin S., Nordin J.P., Sullivan D.J. and Neugebauer-Crawford S. (2000) Rates and mechanisms of oxygen exchanges between sites in the $AlO_4Al_{12}(OH)_{24}(H_2O)_{12}^{7+}$(aq) complex and water: Implications for mineral surface chemistry. *Geochim. Cosmochim. Acta* **64**, 2951-2964.

Chen K., Walker R.J., Rudnick R.L., Gao S., Gaschnig R.M., Puchtel I.S., Tang M. and Hu Z.-C. (2016) Platinum-group element abundances and Re–Os isotopic systematics of the upper continental crust through time: Evidence from glacial diamictites. *Geochim. Cosmochim. Acta* **191**, 1-16.

Cobelo-García A., Turner A. and Millward G.E. (2008) Fractionation and Reactivity of Platinum Group Elements During Estuarine Mixing. *Environmental Science & Technology* **42**, 1096-1101.

Cobelo-García A., Turner A., Millward G.E. and Couceiro F. (2007) Behaviour of palladium(II), platinum(IV), and rhodium(III) in artificial and natural waters: influence of reactor surface and geochemistry on metal recovery. *Anal Chim Acta* **585**, 202-210.

Cobelo-García A., López-Sánchez D.E., Almécija C. and Santos-Echeandía J. (2013) Behavior of platinum during estuarine mixing (Pontevedra Ria, NW Iberian Peninsula). *Mar. Chem.* **150**, 11-18.

Coker W.B., Dunn C.E., Hall G.E.M., Rencz A.N., DiLabio R.N.W., Spirito W.A. and Campbell J.E. (1991) The behaviour of platinum group elements in the surficial environment at Ferguson Lake, N.W.T., Rottenstone Lake, Sask. and Sudbury, Ont., Canada. *J. Geochem. Explor.* **40**, 165-192.

Colombo C., Oates C.J., Monhemius A.J. and Plant J.A. (2008) Complexation of platinum, palladium and rhodium with inorganic ligands in the environment. *Geochem.: Explor. Environ. Anal.* **8**, 91-101.

Deberdt R., Smith N.M., Calderon J.L. and McCall S.K. (2025) Critical minerals lists for low-carbon transitions: Reviewing their structure, objectives, and limitations. *Energy Res. Soc. Sci.* **127**.

Dockrey J., Lindsay M., Mayer K., Beckie R., Norlund K., Warren L. and Southam G. (2014) Acidic Microenvironments in Waste Rock Characterized by Neutral Drainage: Bacteria–Mineral Interactions at Sulfide Surfaces. *Minerals* **4**, 170-190.

Domènech C., Galí S., Villanova-de-Benavent C., Soler J.M. and Proenza J.A. (2017) Reactive transport model of the formation of oxide-type Ni-laterite profiles (Punta Gorda, Moa Bay, Cuba). *Miner. Deposita* **52**, 993-1010.

Domínguez-Carretero D., Proenza J.A., Villanova-de-Benavent C., Aiglsperger T., Tauler E., Rojas-Purón A., Duque N., González-Jiménez J.-M., Garcia-Casco A. and Galí S. (2024) The Geology, Geochemistry, and Mineralogy of the Moa Bay Ni Laterite Mining District, Cuba. *Econ. Geol.* **119**, 1685-1706.

Dzingai T., McFadzean B., Tadie M. and Becker M. (2021) Decoupling the effects of alteration on the mineralogy and flotation performance of Great Dyke PGE ores. *J. S. Afr. Inst. Min. Metall.* **121**, 475-486.

Elding L.I. (1970) The Stepwise Dissociation of the Tetrachloroplatinate(II) Ion in Aqueous Solution VI. Rates of Formation and Equilibria of the Chloro Aqua Complexes of Platinum(II). *Acta Chem. Scand.* **24**, 1527-1540.

Elding L.I. and Leden I. (1966) On the Stepwise Dissociation of the Tetrachloridoplatinate(II) Ion in Aqueous Solution I. Equilibria at 25° *Acta Chem. Scand.* **20**, 706-715.

Elding L.I. and Gustafson L. (1977) Bromide Anation Kinetics for Some Platinum(IV) Bromo Aqua Complexes. *Inorg. Chim. Acta* **22**, 201-207.

Evans D.M. (2002) Potential for bulk mining of oxidized platinum-group element deposits. *Appl. Earth Sci.* **111**, 81-86.

Fandeur D., Juillot F., Morin G., Olivi L., Cognigni A., Webb S.M., Ambrosi J.-P., Fritsch E., Guyot F. and Brown G.E. (2009) XANES Evidence for Oxidation of Cr(III) to Cr(VI) by Mn-Oxides in a Lateritic Regolith Developed on Serpentinized Ultramafic Rocks of New Caledonia. *Environ. Sci. Technol.* **43**, 7384-7390.

Ferreira C.M.H., Pinto I.S.S., Soares E.V. and Soares H.M.V.M. (2015) (Un)suitability of the use of pH buffers in biological, biochemical and environmental studies and their interaction with metal ions – a review. *RSC Adv.* **5**, 30989-31003.

Fuchs W.A. and Rose A.W. (1974) The Geochemical Behavior of Platinum and Palladium in the Weathering Cycle in the Stillwater Complex, Montana. *Econ. Geol.* **69**, 332-346.

Giorgis I., Bonetto S., Giustetto R., Lawane A., Pantet A., Rossetti P., Thomassin J.-H. and Vinai R. (2014) The lateritic profile of Balkouin, Burkina Faso: Geochemistry, mineralogy and genesis. *J. Afr. Earth Sci.* **90**, 31-48.

Giovannini A.L., Bastos Neto A.C., Porto C.G., Pereira V.P., Takehara L., Barbanson L. and Bastos P.H.S. (2017) Mineralogy and geochemistry of laterites from the Morro dos Seis Lagos Nb (Ti, REE) deposit (Amazonas, Brazil). *Ore Geol. Rev.* **88**, 461-480.

Grantham L.F., Elleman T. S. and Martin D.S. (1955) Exchange of Chlorine in Aqueous Systems Containing Chloride and Tetrachloroplatinate(II). *J. Am. Chem. Soc.* **77**, 2965-2971.

Gray D.J., Schorin K.H. and Butt C.R.M. (1996) Mineral associations of platinum and palladium in lateritic regolith, Ora Banda Sill, Western Australia. *J. Geochem. Explor.* **57**, 245-255.

Gröning Ö. and Elding L.I. (1989) Water Exchange of *trans*-Dichlorodiaquaplatinum(II) and Tetraaquaplatinum(II) Studied by an Oxidative-Addition Quenching Technique. Isotopic Shifts and Platinum-195 NMR Chemical Shifts for Mixed Chloro-Aqua Complexes of Platinum(II) and Platinum(IV). *Inorg. Chem.* **28**, 3366-3372.

Hao X., Quach L., Korah J., Spieker W.A. and Regalbuto J.R. (2004) The control of platinum impregnation by PZC alteration of oxides and carbon. *J. Mol. Catal. A.: Chem.* **219**, 97-107.

Hyland E.G., Sheldon N.D., Van der Voo R., Badgley C. and Abrajevitch A. (2015) A new paleoprecipitation proxy based on soil magnetic properties: Implications for expanding paleoclimate reconstructions. *Geol. Soc. Am. Bull.* 10.1130/b31207.1.

Ito A., Otake T., Maulana A., Sanematsu K., Sufriadin and Sato T. (2021) Geochemical constraints on the mobilization of Ni and critical metals in laterite deposits, Sulawesi, Indonesia: A mass-balance approach. *Resour. Geol.* **71**, 255-282.

Jiménez-Martínez J., Anna P. d., Tabuteau H., Turuban R., Borgne T.L. and Méheust Y. (2015) Pore-scale mechanisms for the enhancement of mixing in unsaturated porous media and implications for chemical reactions. *Geophys. Res. Lett.* **42**, 5316-5324.

Johnson R.C., Basolo F. and Pearson R.G. (1962) Base hydrolysis of some chloroammine-platinum(IV) complexes. *J. Inorg. Nucl. Chem.* **24**, 59-71.

Kämpf N. and Schwertmann U. (1983) Goethite and Hematite in a Climosequence in Southern Brazil and their Application in Classification of Kaolinitic Soils. *Geoderma* **29**, 27-39.

Kashiwabara T., Watanabe Y., Ishikawa A., Tokeshi S., Sato H., Ijichi Y., Kikuchi S., Sekizawa O., Nitta K., Uruga T., Hein J.R., Usui A. and Takahashi Y. (2026) Direct speciation of ultra-trace platinum in marine ferromanganese oxides by wavelength-dispersive XAFS. *Chem. Lett.* upag171, doi:10.1093/chemle/upag171.

Kelly S.D., Hesterberg D. and Ravel B. (2008) Analysis of Soils and Minerals Using X-ray Absorption Spectroscopy. In *Methods of Soil Analysis Part 5—Mineralogical Methods* (eds. A. L. Ulery and L. R. Drees). Soil Science of America, Inc., Madison. pp. 387-464.

Koschinsky A., Hein J.R., Kraemer D., Foster A.L., Kuhn T. and Halbach P. (2020) Platinum enrichment and phase associations in marine ferromanganese crusts and nodules based on a multi-method approach. *Chem. Geol.* **539**.

Kubrakova I.V., Fortygin A.V., Lobov S.G., Koshcheeva I.Y., Tyutyunnik O.A. and Mironenko M.V. (2011) Migration of platinum, palladium, and gold in the water systems of platinum deposits. *Geochem. Int.* **49**, 1072-1084.

Ledingham G.J., Fang Y. and Catalano J.G. (2024) Irreversible Trace Metal Binding to Goethite Controlled by the Ion Size. *Environ. Sci. Technol.* **58**, 2007-2016.

Ledingham G.J., Custis A.T., Fang Y. and Catalano J.G. (2025) Short-Term Inhibition and Long-Term Enhancement of Irreversible Trace Metal Binding to Goethite in Multi-Metal Systems. *Environ. Sci. Technol.* **59**, 12302-12313.

Li W., Livi K.J., Xu W., Siebecker M.G., Wang Y., Phillips B.L. and Sparks D.L. (2012) Formation of Crystalline Zn-Al Layered Double Hydroxide Precipitates on γ-Alumina: The Role of Mineral Dissolution. *Environ. Sci. Technol.* **46**, 11670-11677.

Li Z., Sun X., Li D., Liang Y., Li S. and Peng J. (2023) Platinum enrichment in marine ferromanganese oxides: Constraints from surface adsorption behavior on synthetic feroxyhyte (δ-FeOOH). *Chemical Geology* **615**.

Liao J., Li Y., Léger J., Koschinsky A., Dejoie C., Gaillot A.-C., Snigireva I., Giacomelli A., Steinmann S.N., Mathon O. and Manceau A. (2026) Platinum occurs as α-PtO_2 nanoparticles in deep-sea ferromanganese deposits. *Geochim. Cosmochim. Acta* in press.

Lincoln S.F. and Merbach A.E. (1995) Substitution Reactions of Solvated Metal Ions. In *Advances in Inorganic Chemistry* (ed. A. G. Sykes). Academic Press. pp. 1-88.

Locmelis M., Melcher F. and Oberthür T. (2010) Platinum-group element distribution in the oxidized Main Sulfide Zone, Great Dyke, Zimbabwe. *Miner. Deposita* **45**, 93-109.

Long X., Ji J., Barrón V. and Torrent J. (2016) Climatic thresholds for pedogenic iron oxides under aerobic conditions: Processes and their significance in paleoclimate reconstruction. *Quat. Sci. Rev.* **150**, 264-277.

Maeno M.Y., Ohashi H., Yonezu K., Miyazaki A., Okaue Y., Watanabe K., Ishida T., Tokunaga M. and Yokoyama T. (2016) Sorption behavior of the Pt(II) complex anion on manganese dioxide (δ-MnO_2): a model reaction to elucidate the mechanism by which Pt is concentrated into a marine ferromanganese crust. *Miner. Deposita* **51**, 211-218.

Marsh E.E. and Anderson E.D. (2011) *Ni-Co laterite deposits*. U.S. Geological Survey Open-File Report 2011-1259.

Martin D.S. (1967) Anomalies in ligand exchange reactions for platinum(II) complexes. *Inorg. Chim. Acta Rev.* **1**, 87-97.

Mashio A.S., Obata H., Tazoe H., Tsutsumi M., Ferrer i Santos A. and Gamo T. (2016) Dissolved platinum in rainwater, river water and seawater around Tokyo Bay and Otsuchi Bay in Japan. *Estuar. Coast. Shelf Sci.* **180**, 160-167.

McGregor R.G., Blowes D.W., Jambor J.L. and Robertson W.D. (1998) The solid-phase controls on the mobility of heavy metals at the Copper Cliff tailings area, Sudbury, Ontario, Canada. *J. Contam. Hydrol.* **33**, 247-271.

Molekoa M., Avtar R., Kumar P., Minh H. and Kurniawan T. (2019) Hydrogeochemical Assessment of Groundwater Quality of Mokopane Area, Limpopo, South Africa Using Statistical Approach. *Water* **11**, 1891.

Molins S. and Knabner P. (2019) Multiscale Approaches in Reactive Transport Modeling. *Rev. Mineral. Geochem.* **85**, 27-48.

Molins S., Trebotich D., Steefel C.I. and Shen C. (2012) An investigation of the effect of pore scale flow on average geochemical reaction rates using direct numerical simulation. *Water Resour. Res.* **48**.
Mountain B.M. and Wood S.A. (1988) Chemical Controls on the Solubility, Transport, and Deposition of Platinum and Palladium in Hydrothermal Solutions: A Thermodynamic Approach. *Econ. Geol.* **83**, 492-510.
Muñoz-Páez A. and Koningsberger D.C. (1995) Decomposition of the Precursor $[Pt(NH_3)_4](OH)_2$, Genesis and Structure of the Metal-Support Interface of Alumina Supported Platinum Particles: A Structural Study Using TPR, MS, and XAFS Spectroscopy. *J. Phys. Chem.* **99**, 4193-4204.
Myagkiy A., Truche L., Cathelineau M. and Golfier F. (2017) Revealing the conditions of Ni mineralization in the laterite profiles of New Caledonia: Insights from reactive geochemical transport modelling. *Chem. Geol.* **466**, 274-284.
Myagkiy A., Golfier F., Truche L. and Cathelineau M. (2019) Reactive Transport Modeling Applied to Ni Laterite Ore Deposits in New Caledonia: Role of Hydrodynamic Factors and Geological Structures in Ni Mineralization. *Geochem. Geophys. Geosyst.* **20**, 1425-1440.
Newville M. (2013) Larch: An Analysis Package for XAFS and Related Spectroscopies. *J. Phys.: Conf. Ser.* **430**, 012007.
Oberthür T. (2018) The Fate of Platinum-Group Minerals in the Exogenic Environment—From Sulfide Ores via Oxidized Ores into Placers: Case Studies Bushveld Complex, South Africa, and Great Dyke, Zimbabwe. *Minerals* **8**, 581.
Oberthür T., Melcher F., Buchholz P. and Locmelis M. (2013) The oxidized ores of the Main Sulphide Zone, Great Dyke, Zimbabwe: turning resources into minable reserves--mineralogy is the key. *J. S. Afr. Inst. Min. Metall.* **113**, 191-201.
Park C., Fenter P.A., Sturchio N.C. and Regalbuto J.R. (2005) Probing outer-sphere adsorption of aqueous metal complexes at the oxide-water interface with resonant anomalous x-ray reflectivity. *Phys. Rev. Lett.* **94**, 076104.
Parks G.A. (1965) The Isoelectric Points of Solid Oxides, Solid Hydroxides, and Aqueous Hydroxo Complex Systems. *Chem. Rev.* **65**, 177-198.
Ravel B. and Newville M. (2005) ATHENA, ARTEMIS, HEPHAESTUS: data analysis for X-ray absorption spectroscopy using IFEFFIT. *J. Synchrotron Radiat.* **12**, 537-541.
Richens D.T. (1997) *The Chemistry of Aqua Ions*, 1 ed. Wiley, Chichester.
Richens D.T. (2005) Ligand Substitution Reactions at Inorganic Centers. *Chem. Rev.* **105**, 1961-2002.
Roney N., Llados F., Little S.S. and Knaebel D.B. (2004) Toxicological Profile for Ammonia.
Sassani D.C. and Shock E.L. (1998) Solubility and transport of platinum-group elements in supercritical fluids: Summary and estimates of thermodynamic properties for ruthenium, rhodium, palladium, and platinum solids, aqueous ions, and complexes to 1000°C and 5 kbar. *Geochim. Cosmochim. Acta* **62**, 2643-2671.
Scheidegger A.M., Lamble G.M. and Sparks D.L. (1997) Spectroscopic Evidence for the Formation of Mixed-Cation Hydroxide Phases upon Metal Sorption on Clays and Aluminum Oxides. *J. Colloid Interface Sci.* **186**, 118-128.
Scheidegger A.M., Strawn D.G., Lamble G.M. and Sparks D.L. (1998) The kinetics of mixed Ni-Al hydroxide formation on clay and aluminum oxide minerals: A time-resolved XAFS study. *Geochim. Cosmochim. Acta* **62**, 2233-2245.

Schlegel M.L. and Manceau A. (2006) Evidence for the nucleation and epitaxial growth of Zn phyllosilicate on montmorillonite. *Geochim. Cosmochim. Acta* **70**, 901-917.
Schreier M. and Regalbuto J.R. (2004) A fundamental study of Pt tetraammine impregnation of silica 1. The electrostatic nature of platinum adsorption. *J. Catal.* **225**, 190-202.
Schwertmann U. (1971) Transformation of Hematite to Goethite in Soils. *Nature* **232**, 624-625.
Schwertmann U. and Cornell R. M. (2000) *Iron Oxides in the Laboratory: Preparation and Characterization*, 2 ed. Wiley-VCH, Weinheim.
Spieker W.A., Liu J., Hao X., Miller J.T., Kropf A.J. and Regalbuto J.R. (2003) An EXAFS study of the coordination chemistry of hydrogen hexachloroplatinate (IV). *Appl. Catal. A: Gen.* **243**, 53-66.
Stumm W. and Sulzberger B. (1992) The cycling of iron in natural environments: Considerations based on laboratory studies of heterogeneous redox processes. *Geochim. Cosmochim. Acta* **56**, 3233-3257.
Takahashi Y., Minai Y., Ambe S., Makide Y. and Ambe F. (1999) Comparison of adsorption behavior of multiple inorganic ions on kaolinite and silica in the presence of humic acid using the multitracer technique. *Geochim. Cosmochim. Acta* **63**, 815-836.
Tauler E., Galí S., Villanova-de-Benavent C., Chang-Rodríguez A., Núñez-Cambra K., Khazaradze G. and Proenza J.A. (2023) Geochemistry and Mineralogy of the Clay-Type Ni-Laterite Deposit of San Felipe (Camagüey, Cuba). *Minerals* **13**.
Thompson R.C. and Rodgers K.A. (1977) Laterization of the Ultramafic-Gabbro Association at North Cape, Northernmost New Zealand. *J. R. Soc. N. Z.* **7**, 347-377.
Torapava N., Elding L.I., Mandar H., Roosalu K. and Persson I. (2013) Structures of polynuclear complexes of palladium(II) and platinum(II) formed by slow hydrolysis in acidic aqueous solution. *Dalton Trans* **42**, 7755-7760.
Trivedi P. and Axe L. (1999) A Comparison of Strontium Sorption to Hydrous Aluminum, Iron, and Manganese Oxides. *J. Colloid Interface Sci.* **218**, 554-563.
Turner A., Crussell M., Millward G.E., Cobelo-García A. and Fisher A.S. (2006) Adsorption Kinetics of Platinum Group Elements in River Water. *Environ. Sci. Technol.* **40**, 1524-1531.
Wood S.A., Mountain B.M. and Fenlon B.J. (1989) Thermodynamic Constraints on the Solubility of Platinum and Palladium in Hydrothermal Solutions: Reassessment of Hydroxide, Bisulfide, and Ammonia Complexing. *Econ. Geol.* **84**, 2020-2028.
Wood S.A., Mountain B.M. and Pan P. (1992) The Aqueous Geochemistry of Platinum, Palladium, and Gold: Recent Experimental Constraints and a Re-evaluation of Theoretical Predictions. *Canad. Mineral.* **30**, 955-982.
Wright E.G., He X., Flynn E.D., Giammar D.E. and Catalano J.G. (2025) Competitive and cooperative effects of chloride on palladium(II) adsorption to iron (oxyhydr)oxides: Implications for mobility during weathering. *Geochim. Cosmochim. Acta* **391**, 203-217.
Wright E.G., Wang I., Fang Y., Flynn E.D. and Catalano J.G. (2026) Climatic Imprint on Interfacially-Controlled Platinum-Palladium Resources. *PNAS Nexus* **5**, pgag196.
Wu L., Schwederski B.E. and Margerum D.E. (1990) Stepwise Hydrolysis Kinetics of Tetrachloroplatinate(II) in Base. *Inorg. Chem.* **29**, 3578-3584.
Zhang L., Wang M., Wang X., Jiang S. and Yuan Z. (2025) Exploring potential platinum demand-supply dynamics in China during process of energy transition till 2050. *Resour. Conserv. Recycl.* **215**.

Zientek M.L., Loferski P.J., Parks H.L., Schulte R.F. and Seal, R.R., II (2017) Platinum-group elements. In K.J. Schulz, J.H. DeYoung, Jr., R.R. Seal, II, D.C. Bradley (Eds.), Critical Mineral Resources of the United States—Economic and Environmental Geology and Prospects for Future Supply. U.S. Department of the Interior, U.S. Geological Survey.

Supplementary Material for:

Mineral-specific ligand and redox dynamics of adsorbed platinum: Pathway-dependent mobility during terrestrial weathering

Emily G. Wright, Fernanda M. Loza, Elaine D. Flynn, Jeffrey G. Catalano*

Department of Earth, Environmental, and Planetary Sciences, Washington University in St. Louis, Saint Louis, MO 63130, USA

*Corresponding author: catalano@wustl.edu

XRD Pattern Collection Parameters

Mineral suspensions were prepared as described in the main text. After drying a subsample of each suspension overnight in a convection oven (70°C for hematite, 55°C for goethite), the resulting solids were used for characterization of mineralogy (XRD) and BET specific surface area. Prior to surface area analysis (**Table S1**), samples were degassed under vacuum at 100°C (hematite) or room temperature (goethite) for at least 18 hours. XRD patterns were collected to verify no other mineral phases were present (**Fig. S1**). For most batches, XRD pattern collection conditions were the same: 10-90° 2θ, 0.02° step size, and 0.2 second count time. However, H#3 and G#2 were collected with the following conditions: 13-65° 2θ, 0.02° step size, and 0.5 second count time. G#5 was collected from 15 to 65° 2θ, with a 0.02° step size and 0.2 second count time.

Thermodynamic Modeling of Aqueous Pt Speciation

There remains considerable disagreement regarding the stability of many Pt species (e.g., Azaroual et al., 2001, 2003; Byrne, 2003), which makes it challenging to reliably predict Pt speciation quantitatively. However, to assess the possible effects of ligands and changing experimental conditions, we calculated equilibrium aqueous Pt speciation using The Geochemist's Workbench® with an altered version of the standard thermodynamic database

from the pyGeochemCalc Python package (Awolayo and Tutolo, 2022). We added Pt as a new element, with Pt^{2+} as the basis species. We included the stability constants for Pt(II)-OH and Pt(II)-NH_3 species from Wood et al. (1989) and Pt(II)-Cl species from Mountain and Wood (1988). These datasets were chosen because they contained all likely relevant Pt(II) species for our experimental system (excluding the possibility of aqueous Pt-Cl-NH_3 species). Speciation was calculated for 50 μM Pt as a function of pH (4-8) in 10 mM chloride, 10 mM chloride and 0.25 mM ammonia, and 10 mM chloride and 10 mM ammonia (**Fig. 1**). For the chloride-only system, sodium was used as the charge balance. For the mixed chloride-ammonia systems, sodium was set to 10 mM and nitrate was used as the charge balance, after decoupling the NO_3^-/$NH_{3(aq)}$ redox couple.

Preliminary Experiment on Effect of Ammonia on Pt Adsorption

To explore the possible effect of ammonia concentrations on Pt adsorption, a preliminary experiment was conducted at pH 7±0.05 (**Fig. S4**). The experiment was conducted with 30 μM tetraaammine platinum(II) nitrate with 1 g/L goethite and varying ammonia concentrations (0.25-10 mM) added as ammonium nitrate. 1 mM MOPS buffer was added to better control the pH. In order to maintain constant ionic strength, sodium nitrate was added to ensure a constant 10 mM nitrate concentration. A corresponding set of mineral-free controls was also prepared. The experiment was pH adjusted, filtered, and analyzed in the same manner as described in the main text.

EXAFS Fits of Pt Standards

Platinum standards ($Pt(O_5C_5H_7)_2$, $PtCl_4(NH_4)_2$, $PtCl_2$, $PtCl_6(NH_4)_2$, and PtO_2) were fit using the backscattering phase and amplitude functions generated from the modified version of *trans*-

$[PtCl(OH)(NH_3)_2]\cdot H_2O$ (Arpalahti et al., 1994) described in the main text in order to better constrain σ^2 for the first shell paths. All samples were fit with an amplitude reduction factor of 0.94 and using the Fourier transform *k*-range from 3.0 to 12.3 $Å^{-1}$. The Pt-Cl solids ($PtCl_2$, $PtCl_4(NH_4)_2$, $PtCl_6(NH_4)_2$) were fit with a single Pt-Cl path and a more limited range in R-space (1.1-3 Å), since we were not interested in the second shell. Similarly, $Pt(O_5C_5H_7)_2$ was fit from 1.1 to 2.3 Å to avoid fitting second shell features. However, this approach was not possible for PtO_2 due to interference. For PtO_2, we fit the alpha structure (Hoekstra et al., 1971), which consisted of multiple Pt-O paths and a Pt-Pt path; the σ^2 value for the two further Pt-O paths were set to be equal to minimize the number of free parameters. Additionally, we included two multiple scattering paths, Pt-O-Pt-O'-Pt and Pt-O-O'-Pt, where O' represents a distinct O backscatterer. The CN for these paths were set to 6 (the same as the first Pt-O path) and the σ^2 and distance for these paths was set to double that of the first Pt-O path. This PtO_2 spectrum was fit in R-space from 1.1 to 5 Å. The resulting structural model fits well reproduce the main feature in the measured spectra (**Fig. S3**). The σ^2 value for the first shell does not substantially differ between Cl and O neighbors, nor from a shift from Pt(II) to Pt(IV) (**Table S3**). Thus, for fitting our experimental samples, a σ^2 value of 0.0026 $Å^2$ was used for the first shell paths.

Variations in Uptake Between Kinetic Experiments

While the general trend of the kinetic experiments is the same for both shorter- and longer-term kinetic reactors (**Fig. 3,S5**), there are quantitative differences between these separate experiments. The initial rate of uptake was faster in the shorter-term kinetic reactors, particularly for goethite (**Fig. 3,S5**), which can be attributed to differences in experimental design and mass transport rates. For both kinetic experiments, the reactors were stored on a shaker table at 180 rpm. However, even at this speed, goethite particles rapidly settled out of solution within several

minutes. Prior to subsampling, reactors were moved to a stir plate and thoroughly mixed for several minutes. Since the shorter-term reactors were sampled more frequently initially, they were probably more well-mixed, resulting in faster uptake rates.

Table S1. Characterization details for mineral batches used in study.

Batch Name	Mineral[a]	Measured Surface Area (m^2/g)[b]	Corresponding Experiments
H#1	hematite	19.1	pH edge experiments with 10 mM chloride (Pt-Cl stock), 10 mM chloride and 0.25 mM ammonia (Pt-Cl stock)
H#2	hematite	20.5	pH edge experiments with 10 mM chloride and 10 mM ammonia (both Pt stocks), 2 mM chloride (Pt-Cl stock) longer-term kinetic experiments with Pt-Cl stock and 10 mM chloride and 10 mM ammonia (Pt-NH_3 stock)
H#3	hematite	N/A	EXAFS samples HCl-pH4, HCl-d1, HCl-pH8
H#4	hematite	N/A	EXAFS samples HCl-d6, HCl-d13, HCl-d29, HCl-d57, HClN-d1, HClN-d6, HClN-d57
H#5	hematite	19.9	all short-term kinetic experiments
H#6	hematite	22.4	longer-term kinetic experiment with 10 mM ammonia (Pt-NH_3 stock)
G#1	goethite	25.4	all pH edge experiments longer-term kinetic experiments with Pt-Cl stock and 10 mM chloride and 10 mM ammonia (Pt-NH_3 stock)
G#2	goethite	N/A	EXAFS samples GCl-pH4, GCl-d1, GCl-pH8
G#3	goethite	N/A	EXAFS samples GCl-d57, GClN-d1, GClN-d57
G#4	goethite	32.1	all short-term kinetic experiments longer-term kinetic experiment with 10 mM ammonia (Pt-NH_3 stock)
G#5	goethite	28.9	preliminary adsorption experiment testing effect of ammonia (**Fig. S4**)

[a]Mineralogy verified with XRD (see **Fig. S1**).

[b]BET specific surface area. Surface area was not measured for mineral batches that were solely used to prepare EXAFS samples.

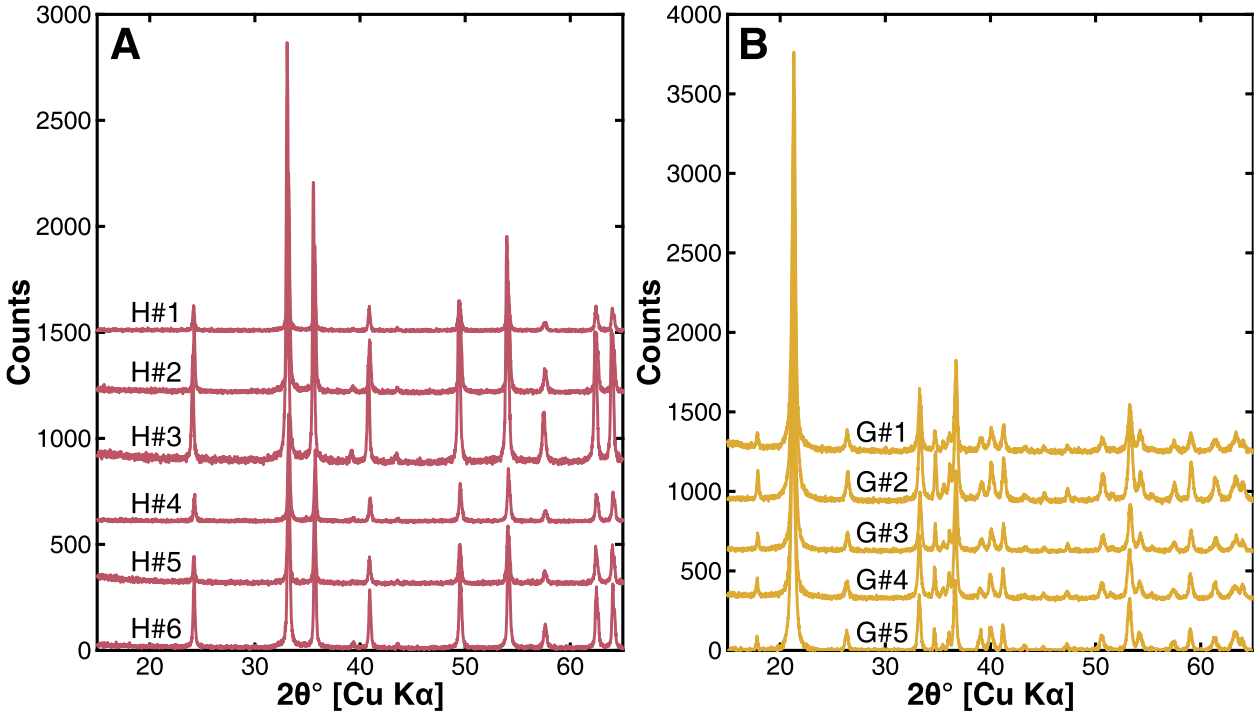

Figure S1. X-ray diffraction patterns of synthesized hematite (**A**) and goethite (**B**) batches used in this study (see **Table S1**).

Table S2. Details regarding XAS sample experimental conditions.

Sample[a]	Mineral Batch	Mineral Loading (g/L)	Sample Volume (mL)	Dissolved Ammonia (mM)	Reaction Time (days)	Final pH	Final Dissolved Pt (µM)	Adsorbed Pt (µmol/g)[b]
HCl-pH4[c]	H#3	8	50	0	1	4.00	22.5	14.6
HCl-pH8	H#3	6	50	0	1	7.99	3.59	22.3
HCl-d1	H#3	6	50	0	1	5.92	8.66	20.4
HCl-d6	H#4	8	50	0	6	5.85	6.71	21.5
HCl-d13	H#4	8	50	0	13	5.84	4.01	22.8
HCl-d29	H#4	8	50	0	29	5.92	2.05	23.5
HCl-d57	H#4	8	50	0	57	5.88	1.38	23.9
HClN-d1	H#4	8	50	10	1	5.96	16.6	18.5
HClN-d6	H#4	8	50	10	6	5.81	10.4	20.5
HClN-d57	H#4	8	50	10	57	5.91	13.9	19.2
GCl-pH4[c]	G#2	3	50	0	1	3.96	10.9	46.0
GCl-pH8	G#2	3	50	0	1	7.90	3.18	40.9
GCl-d1	G#2	3	50	0	1	5.94	3.17	45.1
GCl-d57	G#3	3	50	0	57	6.03	0.66	47.7
GClN-d1	G#3	3	50	10	1	6.02	5.35	42.5
GClN-d57	G#3	3	50	10	57	5.96	1.85	45.5

[a]Names that start with "H" and "G" are hematite and goethite samples, respectively.
[b]Calculated by difference from the target initial Pt concentration, instead of a corresponding mineral-free control.
[c]Samples were previously reported in Wright et al. (2026) but spectra were refit for this project. HCl-pH4 was reported as H10lPt and GCl-pH4 as G10lPt.

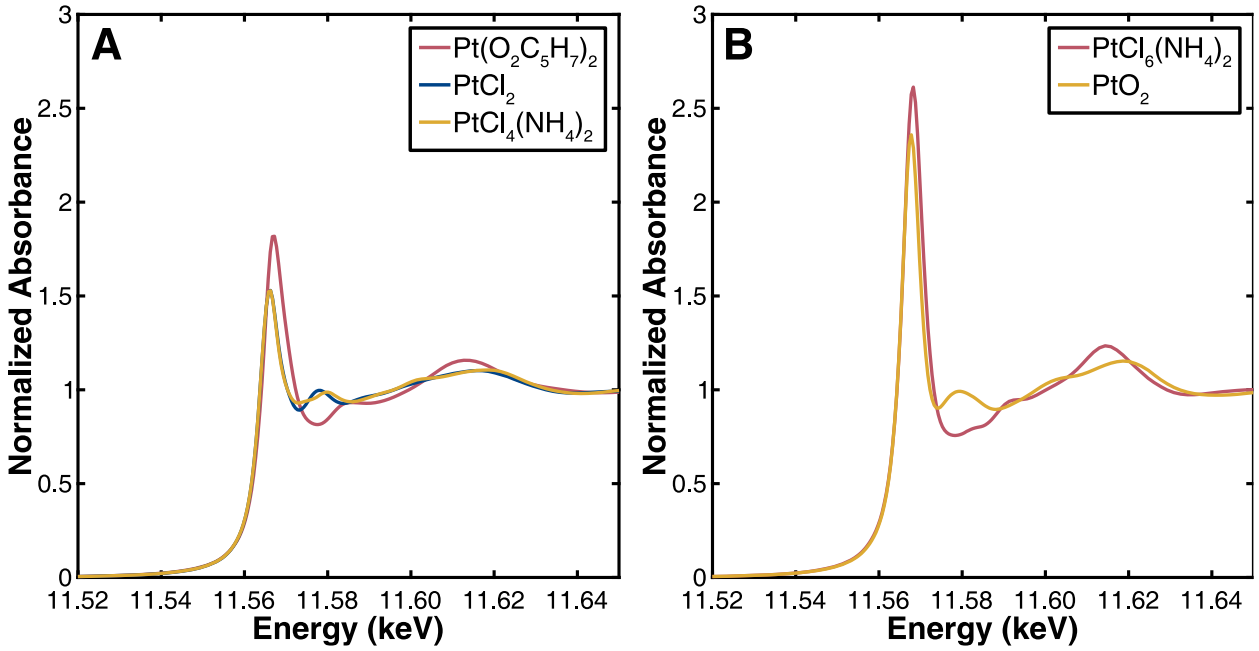

Figure S2. Platinum L_3-edge XANES spectra of Pt(II) (**A**) and Pt(IV) (**B**) standards.

Table S3. Pt L_3-edge EXAFS fitting parameters for reference standards.

Standard	Path	CN[a]	R (Å)[b]	σ^2 (Å^2)[c]	ΔE_0 (eV)[d]	*R* factor[e]	χ_v^{2e}
$PtCl_2$	Pt-Cl	4	2.313(4)[f]	0.0029(2)	13.5(9)	0.008	112.5
$PtCl_4(NH_4)_2$	Pt-Cl	4	2.313(3)	0.0029(1)	13.7(6)	0.003	53.43
$Pt(O_2C_5H_7)_2$	Pt-O	4	1.980(8)	0.0023(6)	12(2)	0.020	2996
$PtCl_6(NH_4)_2$	Pt-Cl	6	2.324(3)	0.0025(1)	15.1(6)	0.004	245.6
PtO_2	Pt-O1	6	2.013(5)	0.0027(4)	12.0(8)	0.021	441.1
	Pt-Pt	6	3.116(5)	0.0037(4)			
	Pt-O2	3	3.7(1)	0.011(9)			
	Pt-O3	6	3.95(7)	0.011			

[a]Coordination number.
[b]Interatomic distance.
[c]Debye-Waller factor.
[d]Energy shift parameter.
[e]Goodness-of-fit parameters (Kelly et al., 2008).
[f]The estimated standard deviations as errors in the last digit are given in parentheses. Parameters constrained during fitting are listed with no uncertainties.

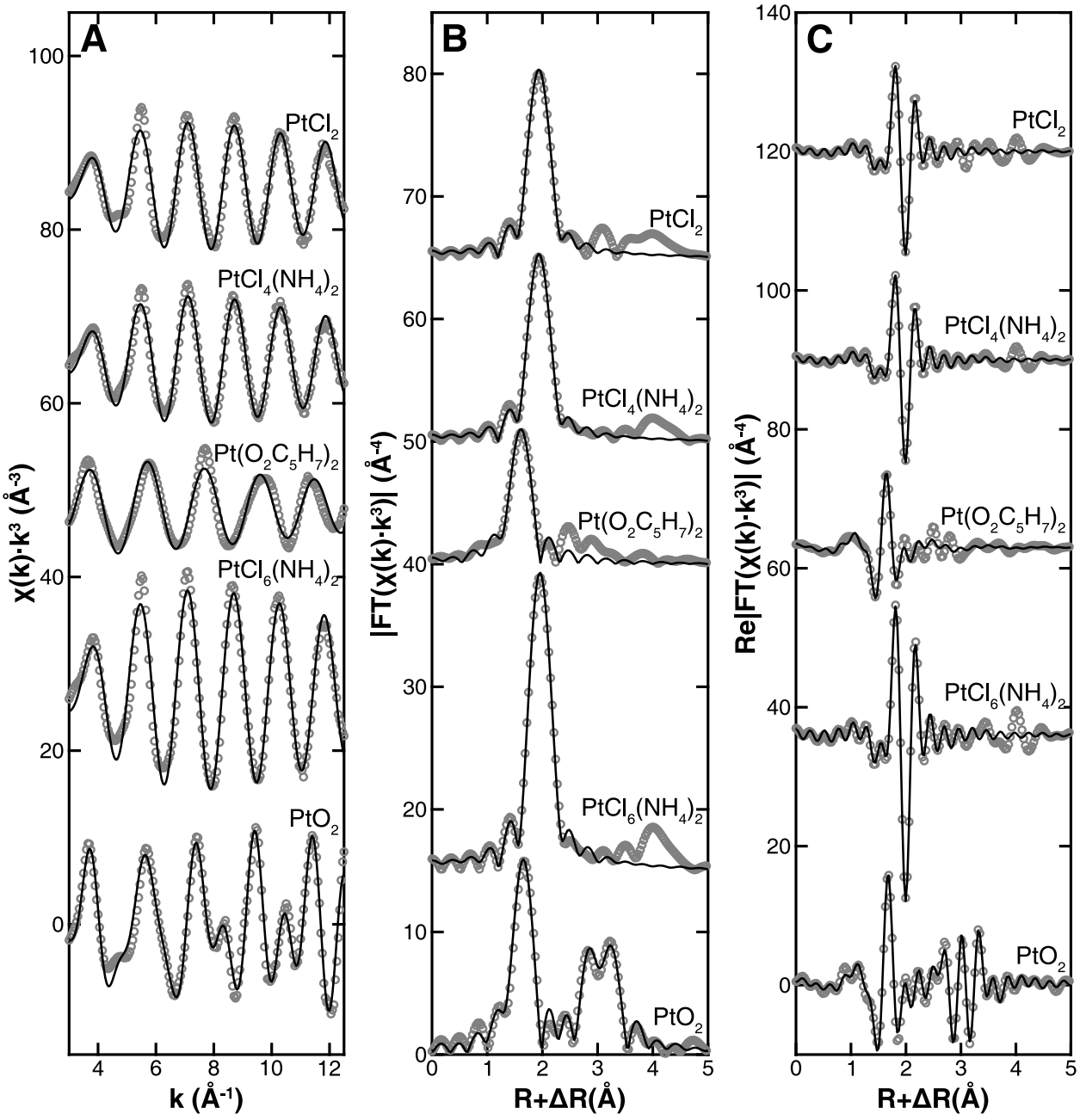

Figure S3. Data (symbols) and structural model fit (line) to reference standard Pt L_3-edge EXAFS spectra (**A**), Fourier transform magnitudes (**B**), and real components of the Fourier transforms (**C**).

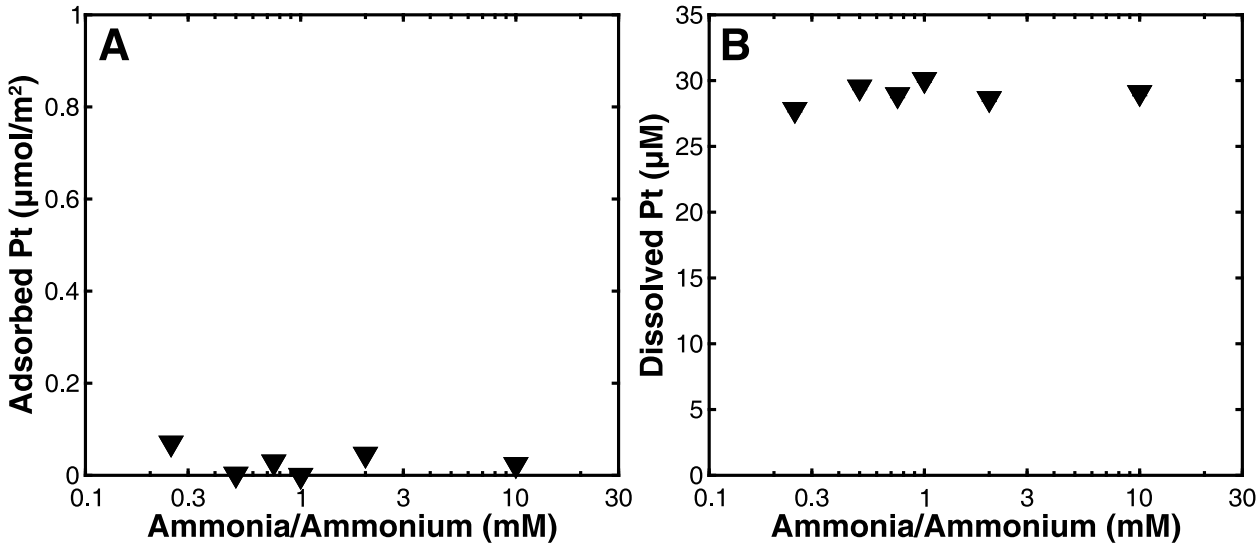

Figure S4. Platinum adsorption (**A**) and remaining dissolved Pt (**B**) to goethite at pH 7.00±0.05 as a function of ammonia concentration after a reaction time of 24 hours. All samples were prepared with Pt-NH_3 complexes with approximately 30 µM Pt.

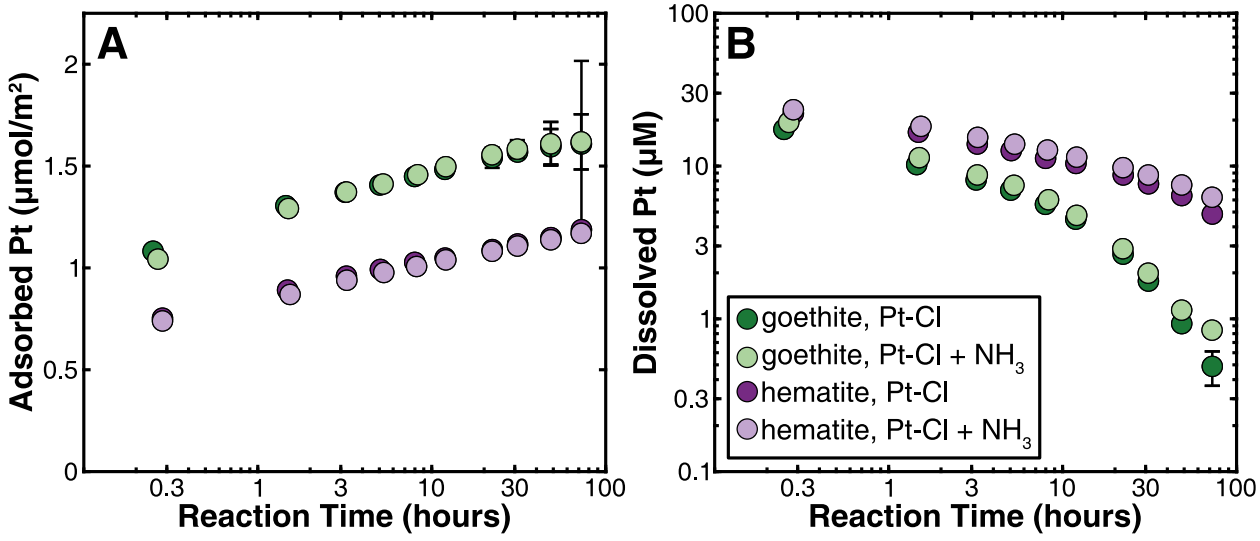

Figure S5. Platinum adsorption to hematite and goethite at pH 6.0±0.2 (**A**) and the corresponding remaining dissolved Pt concentrations (**B**) as a function of reaction time in the shorter-term kinetic reactors. Errors smaller than the symbols are not shown. All reactors shown were prepared with Pt-Cl species and contained either 10 mM chloride or 10 mM chloride and 10 mM ammonia.

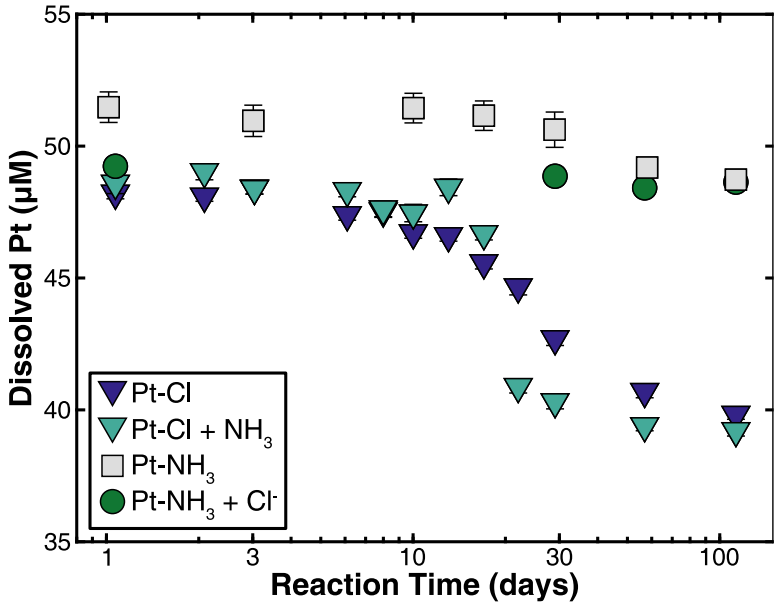

Figure S6. Dissolved Pt in mineral-free reactors as a function of reaction time at pH 6.0±0.2. Reactors were prepared with Pt-Cl or Pt-NH_3 stock and contain 0 or 10 mM chloride and 0 or 10 mM ammonia.

Table S4. Principal component analysis for the EXAFS spectra of Pt adsorbed to hematite.

Component	Variance	Cumulative Variance	IND[a]
1	0.866054	0.866054	0.04591
2	0.084150	0.950205	0.01390
3	0.015866	0.966070	0.01312
4	0.008812	0.974882	0.01452
5	0.005654	0.980537	0.01855
6	0.005172	0.985708	0.02522
7	0.004406	0.990115	0.03912
8	0.003697	0.993812	0.07742
9	0.003446	0.997257	0.25861
10	0.002743	1.000000	-

[a]Indicator value.

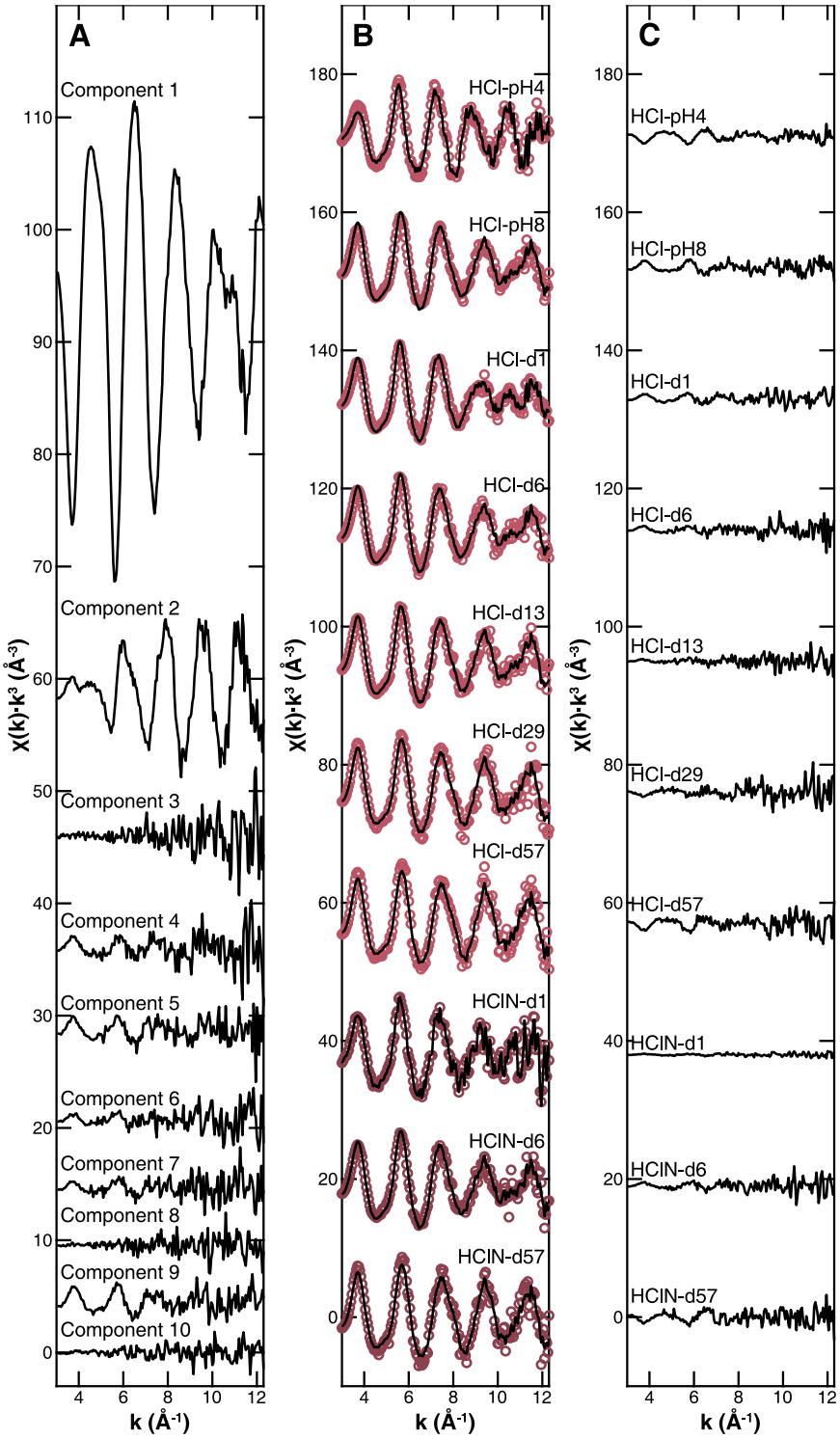

Figure S7. Results of the principal component analysis of the EXAFS spectra of Pt adsorbed to hematite. (**A**) Principal components derived from analysis. (**B**) Reconstruction (line) of the experimental spectra (points) using three principal components. (**C**) Resulting residuals from reconstructions. Detailed sample information is provided in **Tables 1** and **S2.**

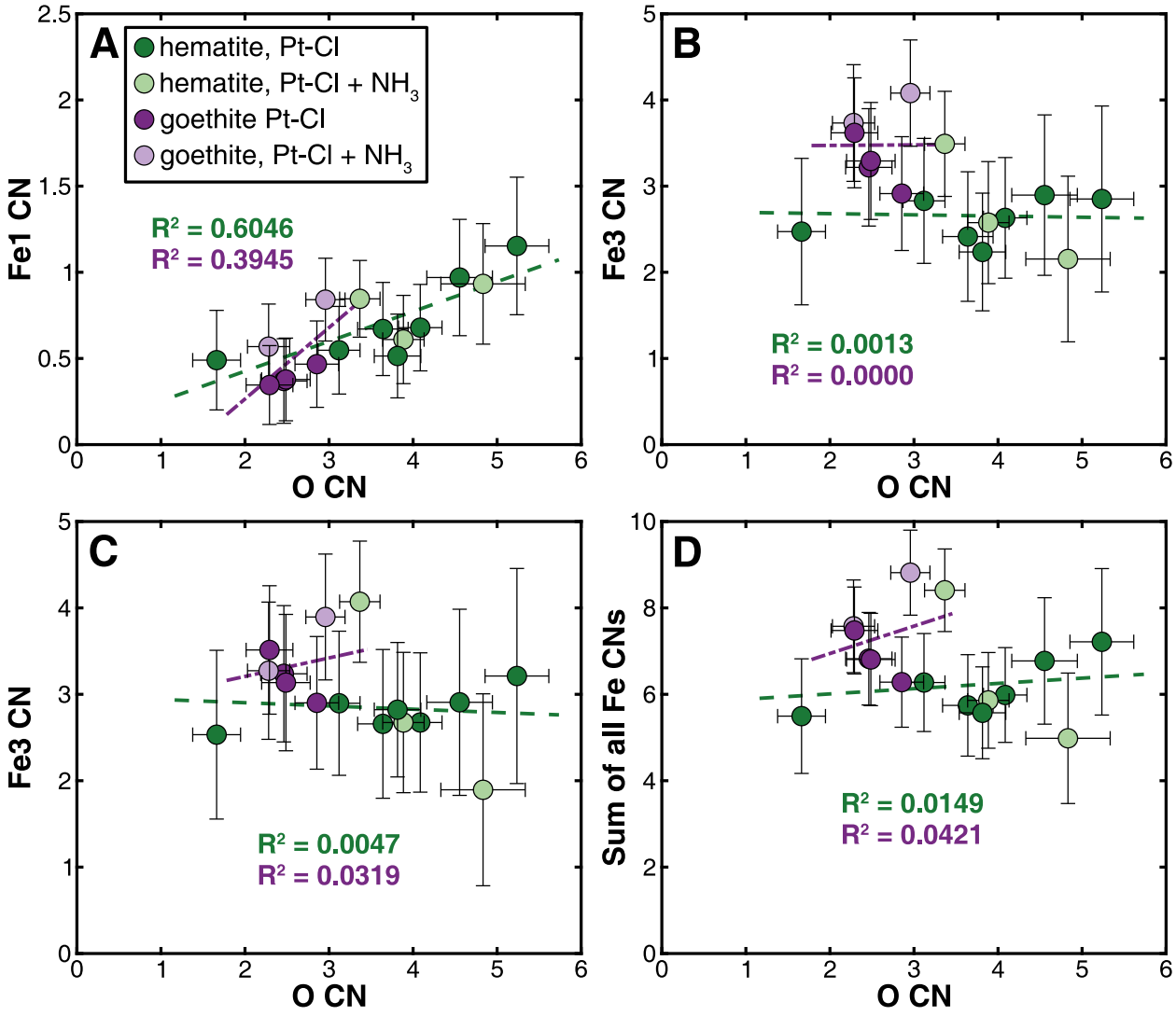

Figure S8. The coordination numbers (CN) for the different Pt-Fe paths versus the O CN for the structural model fits to the EXAFS spectra (see **Tables 1** and **2**), showing the Fe1 neighbor at ~3.07 Å (**A**), the Fe2 neighbor at ~3.68 Å (**B**), the Fe3 neighbor at ~3.87 Å (**C**), and the sum of all Fe paths (**D**). The error for the sum of all Fe CNs was calculated as the square root of the sum of the squared errors for all individual Pt-Fe paths. An unweighted linear regression line and associated R^2 value are shown for all hematite and goethite samples.

Table S5. Alternative Pt L_3-edge EXAFS fitting parameters for previously published pH 4 samples.

Sample[a]	Path	CN[b]	R (Å)[d]	σ^2 (Å^2)[e]	ΔE_0 (eV)[f]	*R* factor[g]	χ_v^{2g}
HCl-pH4	Pd-O	1.8(1)[h]	2.02(1)	0.0012(5)	12.4(9)	0.007	1.91
	Pd-Cl	2.2	2.295(5)	0.0013			
	Pd-Fe1	0.5(2)	3.03(2)	0.005			
	Pd-Fe2	1.8(5)	3.70(1)	0.005			
	Pd-Fe3	1.6(5)	3.90(2)	0.005			
GCl-pH4	Pd-O	2.3(1)	2.02(1)	0.0007(5)	12(1)	0.010	11.37
	Pd-Cl	1.7	2.279(8)	0.0007			
	Pd-Fe1	0.3(2)	3.07(4)	0.005			
	Pd-Fe2	2.8(5)	3.69(1)	0.005			
	Pd-Fe3	2.3(6)	3.90(2)	0.005			

[a]Samples were previously published by Wright et al. (2026). HCl-pH4 was reported as H10lPt and GCl-pH4 as G10lPt. For more sample information, see **Table S2**.
[b]Coordination number.
[c]Interatomic distance.
[d]Debye-Waller factor.
[e]Energy shift parameter.
[f]Goodness-of-fit parameters (Kelly et al., 2008).
[g]The estimated standard deviations as errors in the last digit are given in parentheses. Parameters constrained during fitting are listed with uno uncertainties.
[h]Fits included the following multiple-scattering paths: Pt-Cl-Cl'-Pt, Pt-Cl-Pt-Cl'-Pt, Pt-Cl-Pt-Cl-Pt, Pt-O-O'-Pt, Pt-O-Pt-O'-Pt, and Pt-O-Pt-O-Pt, where Cl'/O' represents a distinct backscatterer. The CNs were set equal to the CN fit to the Pt-Cl/O single paths, with interatomic distances and σ^2 values set as double.

Table S6. Principal component analysis for the EXAFS spectra of Pt adsorbed to goethite.

Component	Variance	Cumulative Variance	IND[a]
1	0.938366	0.938366	0.04970
2	0.033756	0.972123	0.03731
3	0.014182	0.986305	0.04004
4	0.007619	0.993923	0.05434
5	0.003810	0.997733	0.15472
6	0.002267	1.000000	-

[a]Indicator value.

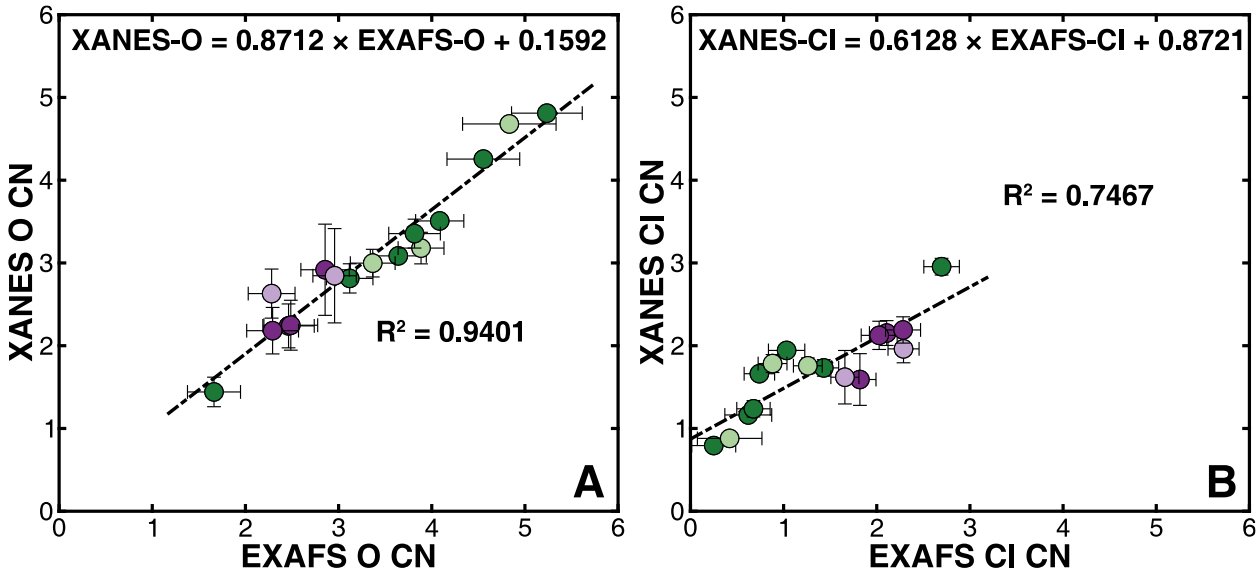

Figure S9. Correlations between the O (**A**) and Cl (**B**) CNs derived from EXAFS structural model fitting compared to XANES LCFs. The unweighted linear regression line and associated R^2 value are shown for all samples.

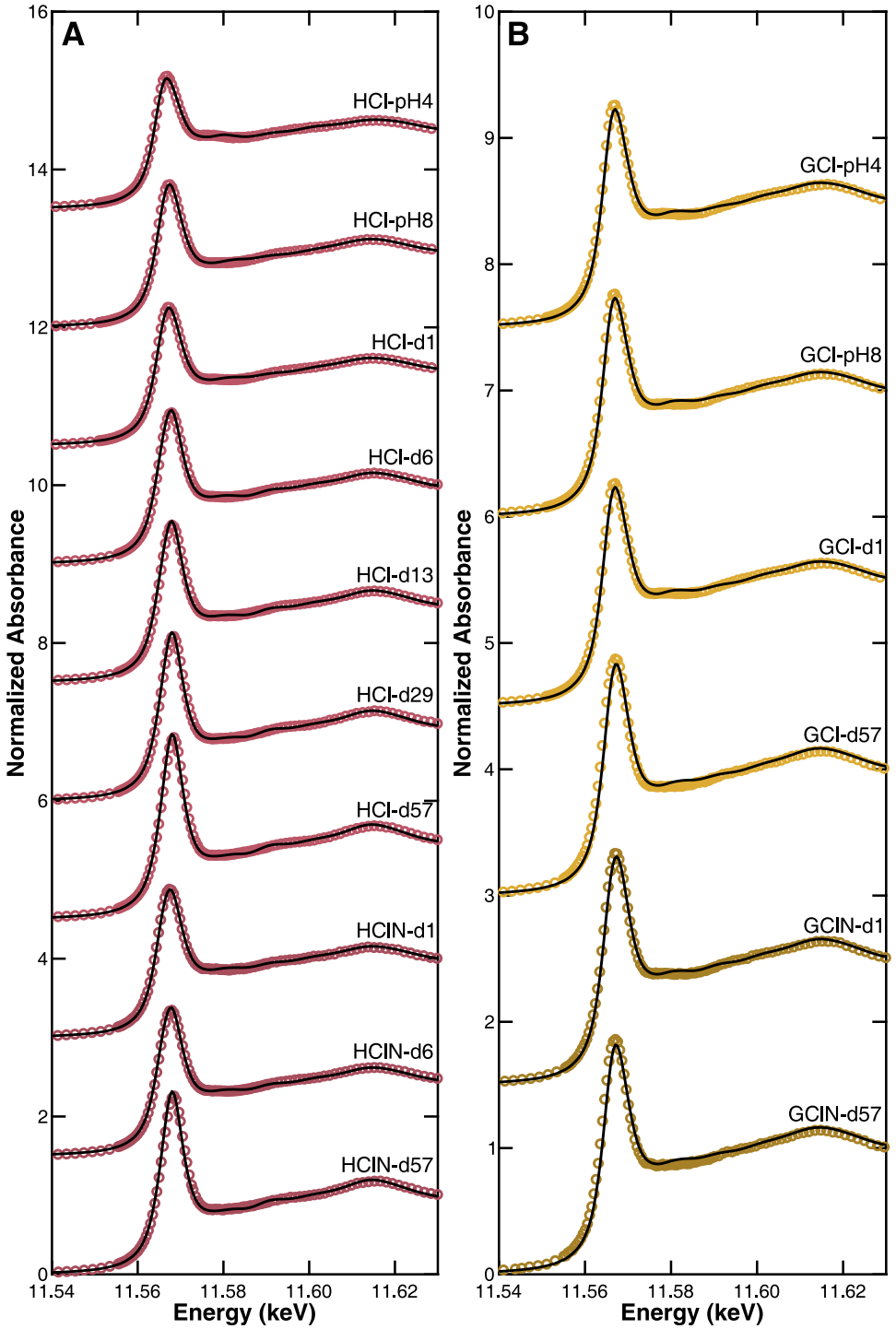

Figure S10. Platinum L_3-edge XANES spectra (symbols) and linear combination fits (solid black lines) of Pt adsorbed to hematite (**A**) and goethite (**B**) at different pH values and for different reaction times. See **Table S2** for more information on samples. LCF results are presented in **Table 3**.

References

Arpalahti J., Sillanpää R. and Mikola M. (1994) Facile Isolation and Crystal Structure Determination of *trans*-[$PtCl(OH)(NH_3)_2$]·H_2O. *J. Chem. Soc., Dalton Trans.* **9**, 1499-1500.

Awolayo A.N. and Tutolo B.M. (2022) PyGeochemCalc: A Python package for geochemical thermodynamic calculations from ambient to deep Earth conditions. *Chem. Geol.* **606**, 120984.

Azaroual M., Romand B., Freyssinet P. and Disnar J.-R. (2001) Solubility of platinum in aqueous solutions at 25°C and pHs 4 to 10 under oxidizing conditions. *Geochim. Cosmochim. Acta* **65**, 4453-4466.

Azaroual M., Romand B., Freyssinet P. and Disnar J.-R. (2003) Response to the comment by R. H. Byrne on "Solubility of platinum in aqueous solutions at 25°C and pHs 4 to 10 under oxidizing conditions" (2001) Geochim. Cosmochim. Acta 65, 4453–4466. *Geochim. Cosmochim. Acta* **67**, 2511-2513.

Byrne R.H. (2003) Comment on "Solubility of platinum in aqueous solutions at 25°C and phs 4 to 10 under oxidizing conditions" by Mohamed Azaroual, Bruno Romand, Philippe Freyssinet, and Jean-Robert Disnar. *Geochim. Cosmochim. Acta* **67**, 2511-2513.

Hoekstra H.R., Siegel S. and Gallagher F.X. (1971) Reaction of Platinum Dioxide with Some Metal Oxides. In *Platinum Group Metals and Compound* (ed. U. V. Rao). American Chemical Society. pp. 39-53.

Kelly S.D., Hesterberg D. and Ravel B. (2008) Analysis of Soils and Minerals Using X-ray Absorption Spectroscopy. In *Methods of Soil Analysis Part 5—Mineralogical Methods* (eds. A. L. Ulery and L. R. Drees). Soil Science of America, Inc., Madison. pp. 387-464.

Mountain B.M. and Wood S.A. (1988) Chemical Controls on the Solubility, Transport, and Deposition of Platinum and Palladium in Hydrothermal Solutions: A Thermodynamic Approach. *Econ. Geol.* **83**, 492-510.

Wood S.A., Mountain B.M. and Fenlon B. J. (1989) Thermodynamic Constraints on the Solubility of Platinum and Palladium in Hydrothermal Solutions: Reassessment of Hydroxide, Bisulfide, and Ammonia Complexing. *Econ. Geol.* **84**, 2020-2028.

Wright E.G., Wang I., Fang Y., Flynn E.D. and Catalano J.G. (2026) Climatic Imprint on Interfacially-Controlled Platinum-Palladium Resources. *PNAS Nexus* **5**, pgag196.